Nanoscale

RSC Publishing

FEATURE ARTICLE

View Article Online
View Journal | View Issue

Cite this: *Nanoscale*, 2013, **5**, 3570

Recent developments and future directions in the growth of nanostructures by van der Waals epitaxy

Muhammad Iqbal Bakti Utama,[a] Qing Zhang,[a] Jun Zhang,[a] Yanwen Yuan,[a] Francisco J. Belarre,[b] Jordi Arbiol[bc] and Qihua Xiong*[ad]

Received 9th December 2012
Accepted 17th February 2013

DOI: 10.1039/c3nr34011b

www.rsc.org/nanoscale

Here we review the characteristics of "van der Waals epitaxy" (vdWE) as an alternative epitaxy mechanism that has been demonstrated as a viable method for circumventing the lattice matching requirements for epitaxial growth. Particular focus is given on the application of vdWE for nonplanar nanostructures. We highlight our works on the vdWE growth of nanowire arrays, tripods, and tetrapods from various semiconductors (ZnO, ZnTe, CdS, CdSe, CdS_xSe_{1-x}, CdTe, and PbS) on muscovite mica substrates, irrespective of the ensuing lattice mismatch. We then address the controllability of the synthesis and the growth mechanism of ZnO nanowires from catalyst-free vdWE in vapor transport growth. As exemplified herein with optical characterizations of ZnO and CdSe nanowires, we show that samples from vdWE may possess properties that are as excellent as those from conventional epitaxy. With our works, we aim to advocate vdWE as a prospective universal growth strategy for nonplanar epitaxial nanostructures.

1 Introduction

van der Waals epitaxy (vdWE) occurs when the epitaxial crystalline material is bound primarily to the substrate by weak van der Waals interactions.[1] Thus, vdWE is different from conventional epitaxy, which has strong chemical bonds connecting the epitaxial material and the substrate at the interface. Various advantageous consequences arise in vdWE due to the difference, including the possibility to grow well-crystallized epitaxial material without any necessity to satisfy lattice matching requirement with the substrate. Recently, there are efforts to revisit and exploit the concept of vdWE due to the increasing research activities in nanotechnology; for example, the emergence of 2D structures with nano- and sub-nanometer thickness such as graphene, MoS_2, and other layered materials necessitates an impeccable material preparation techniques. vdWE is

[a]*Division of Physics and Applied Physics, School of Physical and Mathematical Sciences, Nanyang Technological University, Singapore 637371*
[b]*Institut de Ciencia de Materials de Barcelona, ICMAB-CSIC, E-08193 Bellaterra, CAT, Spain*
[c]*Institució Catalana de Recerca i Estudis Avancats (ICREA), 08010 Barcelona, CAT, Spain*
[d]*Division of Microelectronics, School of Electrical and Electronic Engineering, Nanyang Technological University, Singapore 639798. E-mail: Qihua@ntu.edu.sg*

Muhammad Iqbal Bakti Utama graduated from Nanyang Technological University (NTU), Singapore in 2012 with a BSc degree (1st class Honours) in physics with a minor in mathematics and concentrations in nanotechnology and optical technology. He is currently a research project officer in Professor Qihua Xiong's group at NTU. Areas of his research interests include: synthesis and preparation of II–VI semiconductor nanowires and nanobelts; structural, optical spectroscopy, and electrical transport characterizations of nanostructures; and nanofabrications with e-beam lithography.

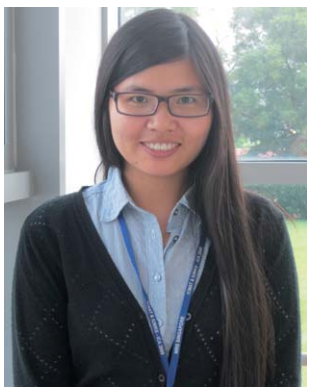

Qing Zhang earned her BS degree in materials physics from University of Science and Technology of China in 2005 and a PhD degree in physics from Tsinghua University in 2011. She is currently a research fellow in Professor Qihua Xiong's group at Nanyang Technological University. Areas of research that she focused on are: optical spectroscopy; optical/excitonic properties of semiconductor; and plasmonics in metallic structures including exciton–plasmon interaction and micro/nano-lasing.

also viewed as a prospective alternative route for the production of nonplanar nanostructures such as nanowire arrays that is not restrained by the availability of suitable substrates. With such an amount of renewed interest in vdWE, a summary on recent advances of the application of vdWE will be instructive for researchers interested in the topic.

In this article, we outline extensively various aspects regarding vdWE. We begin by reviewing the fundamentals and characteristics of conventional heteroepitaxy. We then discuss the concept of vdWE by contrasting its characteristics to those of conventional heteroepitaxy. Particular focus is given on the line of research we conducted on the applications of vdWE to nonplanar nanostructures, where we position our works coherently in the context of the expansion of the applicability of vdWE. Original results are also included in this work, such as the observation of epitaxial tetrapods from various II–VI semiconductors, controlled synthesis and the growth mechanism of ZnO nanowire arrays by catalyst-free vdWE, and optical characterizations of ZnO and CdSe nanowire arrays from vdWE. We end the article with valuable future directions for studies that could endeavor to develop vdWE further.

2 Fundamentals of vdWE

2.1 Conventional heteroepitaxy and mismatch-related defects

Epitaxy (Greek origin, *epi* = above + *taxis* = order) refers to the phenomenon when a crystalline material (referred to as the "overlayer") is grown at the surface of another crystal ("substrate") where the atomic building blocks of the overlayer are arranged in an orderly fashion by consistently following specific orientational crystalline relations with the substrate.[2] According to the material of the substrate, epitaxy can be divided into: (1) *homoepitaxy*, where the substrate is of the same material with the overlayer, and (2) *heteroepitaxy*, when otherwise. On the atomistic level, "conventional" epitaxy (*i.e.*, both homo- and heteroepitaxy) involves chemical bonds at the interface between the overlayer and the substrate. The formation of such bonds can be attributed to the presence of dangling bonds on the clean surface of most crystalline materials, including semiconductors,[1,3] due to the termination of bonds in the bulk for the creation of surfaces. The chemical bonds at the interface force each atom of the overlayer to be paired with a distinct atom of the substrate: the pairing of atoms is responsible for the crystalline ordering in an epitaxial growth, causing the overlayer to mimic the crystalline symmetry of the substrate.

In the description of conventional heteroepitaxy as above, we have assumed that the dangling bonds are not passivated completely by spontaneous processes such as relaxation and reconstruction. Relaxation and reconstruction are the primary mechanisms in which the surface free energy of the new surface can be minimized to achieve a new equilibrium, since the energetics and equilibrium position of atoms close to the surface plane may have changed due to the breaking of the periodicity of the crystal upon the creation of a new clean

Jun Zhang received his PhD degree in Physical-Electronics from Institute of Semiconductors, Chinese Academy of Science, Beijing, China, in 2010. Dr Zhang joined the Professor Qihua Xiong group in May 2010 as a Research Fellow at Nanyang Technological University. His research interests are on Raman and photoluminescence spectroscopy in semiconductor nanostructures. His current research field includes: (1) Raman scattering of 2D layered crystals; (2) surface enhanced Raman spectroscopy; and (3) laser cooling of semiconductors.

Jordi Arbiol graduated in Physics at Universitat de Barcelona (UB) in 1997. He obtained his PhD (PhD Extraordinary Award) in 2001 at UB. He was Assistant Professor at UB. In 2009 he became ICREA Research Professor at Institut de Ciència de Materials de Barcelona, ICMAB-CSIC. He is currently the leader of the Group of Advanced Electron Nanoscopy and Scientific Supervisor of the electron microscopy facilities at ICMAB-CSIC. He is member of the Executive Board of the Spanish Microscopy Society (SME). He has been project Advisor for ANEP, CSIC, ASF, ANPCyT and USP member for the FP7 EU Program I3 ESTEEM2.

Qihua Xiong earned his BS degree in physics from Wuhan University in 1997 and a MS degree from Shanghai Institute of Applied Physics, CAS in 2000. He received a PhD degree in materials science from the Pennsylvania State University in 2006. After three years postdoctoral experience at Harvard University, he joined Nanyang Technological University as a Nanyang assistant professor in 2009. Professor Xiong's research focuses on a various topics in emerging nanomaterials and nanostructures, from fundamental physical properties to applications in nanoelectronics, energy harvesting and biosensing. Recently he also discovered the laser cooling of semiconductors in nanoribbons.

surface in a bulk material. In reconstruction, which is prevalent in semiconductor surfaces, the surface atoms are displaced laterally to change the lattice spacing or even the crystalline symmetry of the surface plane.[4] The incentive of the surface reconstruction in many semiconductors is the reduction of surface dangling bonds; adjacent surface atoms with dangling bonds may create new bonds which thus change the structure of the surface. However, the bonds participating in the reconstruction could still be broken to accommodate new bonds occurring at the surface, since reconstruction can be induced with the presence of adsorbates. Reactivation of dangling bonds due to adsorbates could then enable the formation of new chemical bonds in a conventional heteroepitaxy. Nevertheless, surface reconstruction does not necessarily eliminate the active dangling bonds completely, such as in the case of the Si(111)–7×7 reconstruction that leaves 19 dangling bonds per unit cell.[5]

Chemical bonds connecting the overlayer and the substrate in an epitaxial growth are generally strong enough to modify the cell parameters of the overlayer from those when the overlayer is homonucleated in the freestanding bulk form (contrast Fig. 1a and b). It is particularly evident in heteroepitaxy, where the material difference between the overlayer and substrate would imply a difference in their in-plane lattice parameters (*i.e.*, lattice parameter of planes normal to the interface).

Suppose that the in-plane lattice parameter of the overlayer material in bulk form is a, which is different from that of the substrate, a_s. In heteroepitaxial growth, strong chemical bonds at the heterointerface force the in-plane lattice parameter of the overlayer to match that of the substrate, elastically straining the overlayer crystal in the process. A parameter called "lattice mismatch" is defined to indicate how in-plane lattice parameters of the bulk value of the overlayer material are different from that of the substrate:

$$f = 100\% \times \frac{a_s - a}{a}. \quad (1)$$

Do note that although lattice mismatch and strain in coherent heteroepitaxy share a similar formulation,[2] lattice mismatch is only used to view the overlayer and the substrate as a potential heteroepitaxial system without an *a priori* assumption on how the epitaxy would be formed. Thus, lattice mismatch could be calculated even before the epitaxial growth.

Due to crystal deformation in the overlayer, lattice-mismatched heteroepitaxy causes strain energy to be stored in the system. When the lattice mismatch is relatively small, the first few atomic layers of the overlayer can be *coherently strained* in a one-to-one correspondence with the substrate (Fig. 1b).[2] The amount of the strain energy accumulates along with the increased thickness of the overlayer throughout the growth process. However, the capability of the epitaxial system to store the strain energy is not limitless; Frank and van der Merwe[7] argued that there exists a critical thickness of thin film structure at which the system is no longer able to accommodate the strain. When the thickness of the thin film exceeds a certain critical value, it is energetically more favorable for the system to nucleate defects to relax the strain energy partially (Fig. 1c). Matthews and Blakeslee[8] developed a model to calculate the critical layer thickness, with a conclusion that the critical thickness is negatively correlated with the lattice mismatch of the system: at highly lattice-mismatched heteroepitaxy the critical thickness will be small.

A highly lattice mismatched (>5%) system contains appreciable number of mismatch-related defects in the form of threading dislocations, edge dislocations, or stacking faults close to the heterointerface (Fig. 1d). Defects are deleterious to the performance of devices based on heteroepitaxial systems. The consequence of defects is especially evident in smaller-sized devices, as even a single defect might become a controlling factor of the device performance.[6] Hence, it is important to study strain engineering and minimization of defect nucleation in the heteroepitaxial system, in order to improve their applicability in future technology, which currently exhibits a continuing trend of size-downscaling.

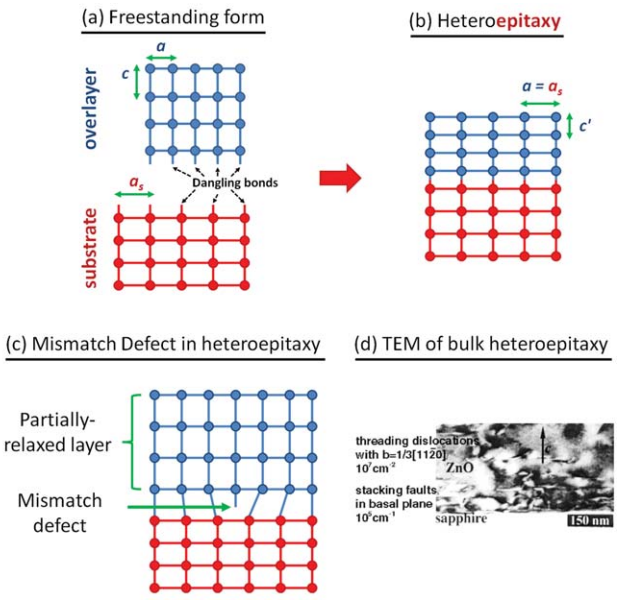

Fig. 1 Conventional epitaxy. (a and b) How heteroepitaxial growth induces strain on the overlayer crystal, modifying the lattice parameters from that in the freestanding bulk form (a). Each circle represents the position of an atom. (c) Defect nucleation (*e.g.*, edge dislocation) as a route to relieve the strain energy in heteroepitaxial growth. Dislocation allows partial elimination of strain at higher height of the overlayer. (d) Cross sectional TEM micrograph of ZnO||sapphire heteroepitaxy, showing threading dislocations and stacking faults due to the lattice mismatch. (Fig. (d) is adapted from ref. 6 with permission.)

2.2 van der Waals epitaxy

There are cases where the concepts of conventional epitaxy are not fully applicable. In 1971, Ying considered that submonolayer gaseous adsorbates on a substrate may be classified into commensurate and incommensurate structures (*i.e.*, when the admolecules are not arranged in a perfect match with the symmetry of the substrate).[9] In 1977, Novaco and McTague published a related scenario on incommensurate structure—also on gaseous adsorbates—where the interactions between the atoms of the overlayer and substrate at the heterointerface are weaker than the interactions between the atoms within the overlayer.[10] The scenario transgresses the assumption of

conventional epitaxy where the heterointerface is connected *via* chemical bonds, similar to how atoms within the overlayer are bound; the interaction of overlayer–substrate and the interaction between the atoms of the overlayer are of comparable strength. Novaco and McTague then argued that the heterointerface with weak overlayer–substrate interaction would behave differently than that with conventional heteroepitaxy: the in-plane lattice parameters at the heterointerface might be incommensurate and the orientation relation between the overlayer–substrate would be unrelated to the crystalline symmetry. However, the relative orientational relation between the adsorbates and the lattices of the substrate, similar to that observed in a typical epitaxial system, still exists for energy minimization. Such a phenomenon is called "*incommensurate epitaxy*".

In 1984, Koma *et al.* reported a phenomenon similar to incommensurate epitaxy using Se/Te and $NbSe_2/MoS_2$ heteroepitaxial crystals as case studies.[1] They suggested that the heteroepitaxy could be bound by the relatively weak van der Waals interactions instead of the stronger chemical bonds. The weakly bound heterointerface cannot strain the first few layers of the overlayer crystal significantly and the nucleation of defects can be prevented even when a large lattice mismatch is present. The term "vdWE" is coined to refer to systems exhibiting such properties.

To allow the growth *via* vdWE instead of *via* conventional heteroepitaxy, Koma and co-workers originally suggested the usage of overlayers and substrates from materials whose surface is free of active dangling bonds,[1,3,11] such as layered materials.[12] The atoms within a layer of layered materials are bound by chemical bonds. However, adjacent layers are connected only by weak van der Waals attractions, which is the reason why layered materials can be cleaved/exfoliated with ease. A freshly cleaved face of a layered material is typically free of dangling bonds. As an example, the absence of dangling bonds in muscovite mica also prevents any occurrence of surface reconstruction, such that the surface of as-exfoliated muscovite is stable and the mean unit cell dimensions at the surface are nearly equal to that of bulk value.[13] The absence of dangling bonds also makes the surface of layered materials relatively inert, not having the tendency to form chemical bonds required for conventional heteroepitaxy. Thus, layered materials (typically referred to as quasi-2D materials to contrast with the bulk, which is 3D) are appropriate for vdWE.

In this work, we have distinguished van der Waals interactions and other chemical (*i.e.*, covalent, metallic, and ionic) bonds, although van der Waals interaction could indeed be considered as a chemical bond as well—or "secondary chemical bond" to be precise, since van der Waals bonds are commonly weak and intermolecular/interionic.[14] But, unlike other chemical bonds, the origin of van der Waals bonds is the Coulombic interactions between the dipole moments from ionic or molecular species involved in the bonds. Thus, a van der Waals bond is based purely on physical force; there is no transfer or sharing of electrons between ions or molecules that change the electronic configuration of the interacting species as is the case in covalent, metallic, and ionic bonds.

In the 1990s, the vdWE concept was expanded to various other materials and corroborated by numerous researchers, including Koma with co-workers (University of Tokyo) and Jaegermann with co-workers (previously at the Hahn-Meitner Institute). It was determined that only either the substrate or the overlayer needs to be of layered materials in order to recruit the vdWE mechanism. Fig. 2 shows the possibilities that have arisen for overlayer–substrate combination. Aside from the growth of layered materials on another layered materials (Fig. 2a), bulk substrates can still be utilized when the top surface is adequately passivated[16,17] (Fig. 2b). In addition, the growth of bulk materials by vdWE may also be achieved, as shown with the growth of CdS film on $MoTe_2$ substrate[18] or CdTe on MoS_2 substrate[19] (Fig. 2c). In all scenarios in Fig. 2, notice the absence of chemical bonds across the interface and the incommensurateness of the in-plane lattice constants between the overlayer and the substrate.

Very recently, vdWE has been applied in the growth of non-continuous nanostructures such as nanoflakes and nanosheets by involving substrates or overlayers of current interest. Instances of such recent reports containing attribution to van der Waals epitaxial growth include: quantum dots of ZnSe on GaSe;[20] topological insulating nanoflakes (Bi_2Se_3 on graphene,[21,22] Bi_2Te_3 on mica,[23,24] and Bi_2Te_2Se on h-BN[25]); graphene flakes on h-BN[26] or on mica;[27] and MoS_2 flakes on graphene.[28] A report on the production of ZnO nanoflakes on mica is also noted in this article (Fig. 13). Although van der Waals epitaxy was historically developed for planar structures, application of vdWE for the growth of nonplanar nanostructures is also gaining steady research attention. We devote Section 3–5 in this article to discuss vdWE in nonplanar nanostructures in more detail.

2.3 Characteristics and characterization techniques relevant to vdWE

We list the characteristics of the system prepared with vdWE as follows:[1,29–31]

(1) In epitaxial growth, the overlayer with vdWE displays a consistent orientational crystalline relation with the substrate.

(2) The overlayer with vdWE exhibits incommensurate/incoherent in-plane lattices at the heterointerface. Thus, vdWE is dissimilar to conventional heteroepitaxy which is coherent,

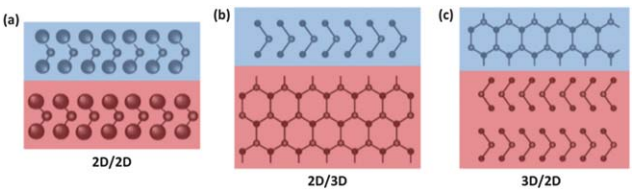

Fig. 2 Illustration of a lattice-mismatched heterointerface in vdWE. vdWE requires that either the substrate and/or the overlayer to be free of dangling bonds, which is satisfied by using layered (2D) materials—instead of bulk (3D) materials—as the overlayer and/or the substrate. Three possible overlayer–substrate scenarios are shown: (a) 2D overlayer on 2D substrate (2D/2D), (b) 2D/3D, and (c) 3D/2D. The red (blue) shading denotes the atoms of the substrate (overlayer). (Adapted from ref. 15 with permission.)

i.e., atoms of the overlayer at the heterointerface are mapped towards atoms of the substrate.

(3) vdWE allows the overlayer to show no excessive strain, allowing the overlayer to be almost perfectly relaxed, even from the heterointerface. Consequently, the in-plane lattice parameters of the overlayer in vdWE will be very close to that of the theoretical bulk value.

(4) vdWE circumvents the strict requirement of conventional heteroepitaxy on the part of the substrate, allowing the growth of compounds with a large lattice mismatch and different crystalline symmetry to that of the substrate. Thus, it is possible to grow epitaxial structures from many different compounds into crystals without defects and buffer layers on a van der Waals substrate.

It is reasonable to discount conventional heteroepitaxy when the above characteristics are present on an epitaxial system, particularly since (conventional) epitaxy and vdWE are the two most prevalent mechanisms to explain the epitaxy-like ordering of overlayer crystals. We remark that the van der Waals interaction between the base of the overlayer and the top surface of the substrate—however weak—should occur in any heterointerface, although the stronger chemical bonds are more dominant in a conventional heteroepitaxy. Similar to physisorption, the adherence of an overlayer material to a substrate may form induced dipoles that would be responsible for vdWE when chemical bonds are absent.

vdWE is an interfacial phenomenon. Hence, surface-sensitive experimental techniques are helpful in assessing the characteristics of the epitaxy within a sample. To argue that an epitaxial growth could be attributed to the vdWE, one could use the idea that chemical bonds are not the dominant factor in mediating the heterointerface in vdWE. In this regard, data from spectroscopic techniques that could probe the chemical binding events—or the absence thereof—are indeed informative. For example, Koma and co-workers collected spectra of low-energy electron loss spectroscopy (LEELS) from freshly cleaved layered substrates with various primary electron energies.[1,11] Since the spectra at low primary energy are similar to those at higher energy and there are no peaks with energy loss that could be ascribed to surface dangling bonds, they concluded that such substrates have no active dangling bonds and should not form chemical bonds with the overlayer during epitaxial growth. To characterize the resulting sample, X-ray and ultraviolet photoemission spectroscopy (XPS and UPS, respectively) could be used to probe the valence and core-level electrons of the overlayer and the substrate. Jaegermann and co-workers reported thickness-dependence studies of overlayers grown with molecular beam epitaxy (MBE).[32,33] vdWE is implied when the spectrum from a thin overlayer (<10 Å) with low coverage is similar to that from thicker overlayers and there is no considerable peak shift or broadening in XPS/UPS spectra, suggesting that the heterointerface is nonreactive.

Other relevant characterization, such as diffractometry, inspects the crystallization of the heterointerface. In-plane lattice parameters of the overlayer at subnanometer thickness and submonolayer coverage can be extracted from reflection high-energy electron diffraction (RHEED) pattern and compared to that at much higher thickness.[1] A similar idea could also be executed with low-energy electron diffraction (LEED).[32,33] In vdWE, it is expected that the in-plane lattice parameters of the overlayer at submonolayer thickness will be similar to the intrinsic bulk value.

Nonplanar nanostructures not grown with MBE are relatively more difficult to characterize. Characterization of planar thin film structures (*e.g.*, XPS, UPS, RHEED, LEED) could be performed *in situ* during the growth process with MBE, as no specialized sample preparation is necessary. XPS and UPS have only a few nanometers probing-depth, such that sample thinning is required. However, the deposition of protective materials onto the sample might be needed during sample thinning, which in turn may complicate the analysis for XPS and UPS. As an alternative to study vdWE in nonplanar nanostructures, the heterointerface could be imaged with high resolution transmission electron microscopy (HRTEM).[30,34] Related analyses could be performed at the heterointerface, such as strain mapping to observe the smallness of the strain and Fourier-filtering to observe the incommensurateness of the in-plane lattices. Under HRTEM, selected area electron diffraction (SAED) or power spectra could be performed to substitute for LEED/RHEED.[30] Characterizations of nonplanar nanostructures are detailed in Section 3.2.2. Association with vdWE may also be done by indirect argument from the intentional usage of substrates known to manifest vdWE (*e.g.*, layered materials such as muscovite mica) and the presence of considerable lattice mismatch with the grown material.[31,35] When the as-grown materials exhibit the characteristics of epitaxy with well-crystallized growth, as verified by HRTEM, scanning electron microscopy (SEM), X-ray powder diffraction (XRD) and related complementary techniques, there is a case for arguing convincingly that vdWE has occurred.

3 Recent applications of vdWE: the growth of epitaxial nonplanar nanostructures

We define "epitaxial nonplanar nanostructures" as epitaxial structures of nanometer size-scale that have extended appendages/protrusions that are not adhered to the substrate. Various technologically relevant nanostructures are included in this class of material: for example, nonplanar nanostructures with quasi-one-dimensionality (1D) such as nanowire arrays are prospective in various applications in electronics, photonics, and optoelectronics.[36–41] However, since the majority of studies on the applications of vdWE were focused on planar structures (*e.g.*, thin films, flakes, platelets), applications in nonplanar nanostructures have not been properly addressed despite their immediate interest until very recently.

3.1 Why the need of vdWE for nonplanar nanostructures?

3.1.1 Heteroepitaxial nanowire array. In discussing the importance to investigate the applicability of vdWE, consider the growth of nanowire arrays, which are the archetype of nonplanar nanostructures. One of the most direct and commonly used method to produce vertical alignment of

nanowires into an array is *via* an epitaxial growth atop a crystalline substrate. However, achieving epitaxy is not a trivial process due to the unwanted formation of defects on the nanowire during the crystallization when the lattice mismatch of the system is large. Similar to that in bulk film, the growth of a well-crystallized nanowire array with conventional epitaxy necessitates that the substrate has similar in-plane lattice parameters and crystalline symmetry to that of the nanowire material.

Admittedly, theoretical and experimental works have shown that nanowires possess a better ability than thin film structure in accommodating lattice mismatch, and thus elastic strain.[42,44,45] Ertekin *et al.* proposed a theoretical model to explain the phenomenon of a defect-free heterointerface of nanowire heterostructures even when a large lattice mismatch is present.[45] The model—also applicable to a heteroepitaxial nanowire array on a bulk substrate—posits that the small diameter of nanowires allows the strain to be relieved laterally, unlike the situation in a thin film structure which has an extended lateral size. As a result, the critical height/thickness that can be achieved by the nanowire array prior to defect nucleation is larger than that of the thin film counterpart with an identical lattice mismatch and material.

Glas supported the calculation of Ertekin *et al.* by showing that the mismatch-dependent critical thickness of nanowire is increased as the radius of the nanowire is reduced (Fig. 3a).[42] Furthermore, Glas also calculated that there could exist a critical radius of nanowire below which the critical thickness approaches infinity (Fig. 3b). An immediate implication of the calculation would be that nanowires with radii below the critical radius would not nucleate mismatch-related defects on the crystal. Despite the significant advantage of the lateral relaxation, it is evident from Fig. 3a that the lateral relaxation capability of nanowire arrays is yet again still very limited. For example, the typical size of an epitaxial GaAs nanowire grown from a vapour-based synthesis method is around 50–100 nm in radius and 1–3 μm, or even up to 10 μm, in length.[46–48] Thus, a completely defect-free nanowire array would require epitaxial growth on substrates with a lattice mismatch of less than 3%. The existence of a critical diameter prior to defect nucleations in nanowires is still widely believed with new reports published to elaborate the subject by considering various other effects, such as variations in nanowire geometry or the elasticity of the substrate.[49,50] Meanwhile, the experimental observation of a mismatch-dependent critical diameter in nanowires was reported by Chuang *et al.*[51] Aside being grown epitaxially with good crystallinity, nanowires smaller than the critical diameter exhibit intense PL with a narrow linewidth.

Regardless of the existence of a critical diameter, it is true that a nanowire array might still be produced epitaxially. For instance, there are reports of direct III–V nanowire array growth on an Si chip, which have appreciable mismatch.[43,52] The nanowires could still grow epitaxially with good morphology as observed *via* SEM/TEM even when the diameter is larger than the critical diameter. However, such nanowires usually produced defects and mismatch dislocations that are localized at the heterointerface, as the lattice of the nanowire still needs to accommodate the strain due to the mismatch to achieve a coherent growth.[43,53] A representative cross-sectional HRTEM image of heteroepitaxial InAs nanowire that is on Si from the work of Tomioka *et al.* which is given in Fig. 3c. Meanwhile, Fig. 3d shows a strain mapping of the InAs–Si cross-section

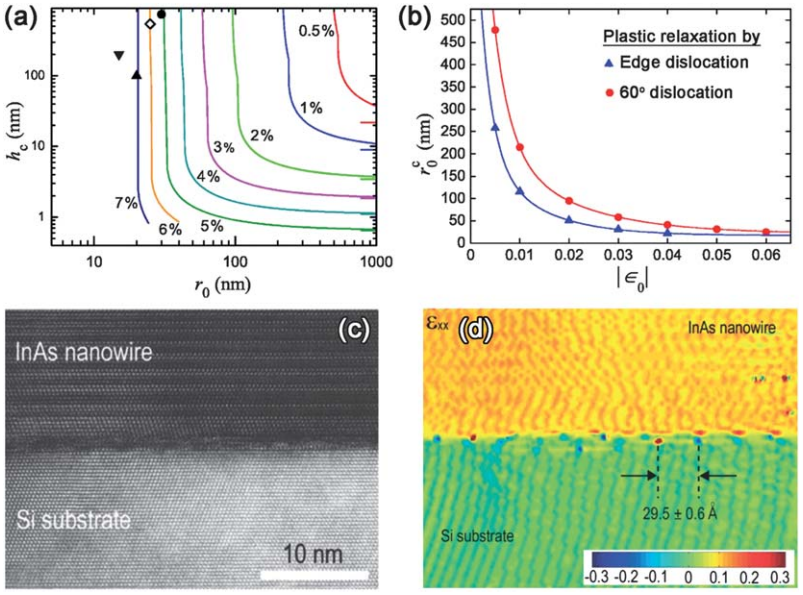

Fig. 3 Accommodation of strain in an heteroepitaxial nanowire array. (a) The theoretical critical thickness (h_c) of a nanowire as a function of the radius of the nanowire (r_0) and the lattice mismatch of the nanowire–substrate (the variously colored curves), suitable for GaAs and a good approximation for other semiconductors. The data points represent experimental results. (b) The critical radius at which the critical thickness approaches infinity, as a function of lattice mismatch. (c) Cross-sectional HRTEM of an epitaxial InAs nanowire on Si (111), with 11.6% mismatch. (d) In-plane strain mapping of the image in (b), showing localization of strains at the heterointerface in the form of mismatch dislocations. (Fig. (a) and (b) are adapted from ref. 42 and Fig. (c) and (d) are adapted from ref. 43 with permission.)

which identifies the presence of periodic strains due to mismatch dislocations.[43] Similar to the case in bulk systems, the mismatch defects and dislocations will affect negatively the application and performance of nanowire array in devices. For example, crystallographic defects are recognized to be a challenge for the integration of nanowire arrays in vertical nanoscale transistors.[54] As another example, mismatch defects in InAs nanowire arrays on Si induce electronic trap states which degrade the switching characteristics and performance of heterojunction tunnel diodes based on this system.[55] Meanwhile, mismatch defects are not an issue in a vdWE nanowire array since the lattice is relaxed even from the heterointerface due to the incommensurateness of the epitaxy,[30] such that mismatch defects can be avoided.

The limitation of substrate for well-crystallized epitaxy limits the applicability of heteroepitaxial growth, including in nanowire arrays. It is not always possible to obtain a suitable substrate (*e.g.*, due to the commercial unavailability of the substrate and/or the difficulty to form a suitable material into a large single crystal as a substrate) with lattice matching and similarity in crystalline symmetry to the nanowire material. Consequently, multitudes of compounds are rarely prepared in the form of epitaxial nanowire arrays. Technological exploration utilizing the nanowire array structure is restrained, since many of the interesting material properties unique to specific compounds cannot be harvested. As such, the exploration of nanowire arrays is therefore presently limited only to a few substrate–compound combinations, such as homoepitaxy.

We acknowledge that the conventional heteroepitaxy of a nanowire array has a very strong applicability in technology due to the possibility to use materials (*e.g.*, Si substrate) that are compatible with established semiconductor processing in industry. The conventional heteroepitaxy of nanowires is also very dependable in many different cases, especially for systems with negligible mismatch and nanowire arrays with a size below the critical diameter. However, conventional heteroepitaxy is limited in very highly lattice mismatched systems and other growth alternatives must be considered to satisfy the niche of achieving a defect-free system in a highly mismatched material; we believe that such a niche is where vdWE could have a strong prospective role.

3.1.2 Buffer layer in lattice-mismatched nanowire arrays. As one possible manifestation of the strain-related defects in highly lattice-mismatched epitaxy of nanowire arrays, it is common for the nanowires to create a form of intermediate structure connecting the nanowires and the substrate. The buffer layer, or as it is also commonly called, the pseudomorphic layer or wetting layer, is an instance of the intermediate structures that are featured prominently at the base of the nanowires. Formation of a buffer layer is a well-known mechanism of strain relaxation in heteroepitaxial structures,[2] including nanowires and crystals in Stranski–Krastanov growth. The extent of such buffer layer manifestation onto the base of the nanowires thus depends on how large is the strain energy to be released, which is a function of nanowire–substrate lattice mismatch and nanowire size, among other factors. As such, the appearance of a buffer layer in nanowires and other nanostructures may also range from an elaborate network of thin films for highly mismatched system to an evident bulging or an intermediate structure only at the base of a wire.[56] A buffer layer can be observed in the electron micrographs displayed in works on nanowire arrays from semiconductors, including ZnO on *a*-sapphire[57] and GaN substrate,[58] GaN on sapphire,[59] InAs on GaAs,[60] and III–V nanowires on an Si substrate.[61] The presence of a buffer layer in samples from various nanowires suggests that the buffer layer structure is a general strain relaxation mechanism that is not unique only to a specific compound. However, as the emergence of the buffer layer is strongly dependent on the strain to be relaxed, structures with a very low amount of strain and a relatively small lattice mismatch may not show an obvious presence of buffer layer at the base of the nanostructure; it is possible that the strain due to lattice mismatch in the system is large enough such that the nanowires nucleate crystalline defects directly in the first few monolayers above the heterointerface (*c.f.*, Fig. 3c and d).

The buffer layer with which we are concerned herein is one that is *spontaneously* formed at the heterointerface during the growth, not one that is intentionally deposited prior to growth. Fig. 4 shows electron micrographs of the buffer layer at the base of ZnO nanowire array on GaN, delineating the typical appearance of buffer layer. Since it is present at the heterointerface, the buffer layer may act as the container of elastic strain due to the lattice mismatch. As a result, besides being observed to be strained,[62] the buffer layer may also be rich in crystalline defects (see Fig. 4c and d).[58] The nucleation of defects in the buffer layer allow the relaxation of the strain of the system, while the rest of the nanowire segment above the buffer layer may continue to grow without strain and defects. Generally, the buffer layer due to strain will be of identical composition to that of the nanowire. The growth of the nanowire array with a buffer layer can thus be regarded as homoepitaxial growth of nanowire array *on* the buffer layer.

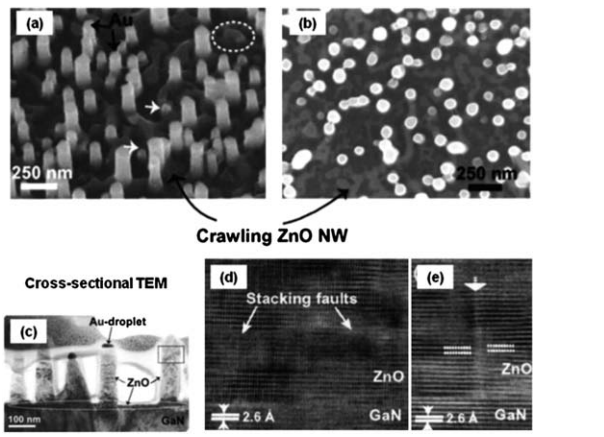

Fig. 4 Buffer layer in ZnO nanowire arrays on a GaN substrate, which implicates a 2% lattice mismatch. (a and b) SEM images in (a) titled view and (b) top view. The buffer layer appears as a "crawling" structure close to the base of the nanowires. (c) Low magnification cross-sectional TEM image of the sample. (d and e) HRTEM images at the ZnO–GaN interface, *i.e.*, at the buffer layer region. The ZnO buffer layer shows crystalline defects and imperfections such as stacking faults which are not normally observed on the stable ZnO wurtzite phase. (Adapted from ref. 58 with permission.)

Buffer layers in nanowire arrays can be viewed as a form of parasitic growth, considering that a buffer layer is also a byproduct of the growth that populates the sample along with the specific nanostructures that are intentionally being produced. Thus, buffer layers—and parasitic crystals in general—will affect (usually, negatively) the overall performance of devices and applications of the sample. However, the term "buffer layer" and "parasitic growth" are not equivalent, given that there are other forms of parasitic crystals which originate from mechanisms other than accommodation of strain at the heterointerface; unlike buffer layer, such parasitic crystals may exist independently from the base of nanowire arrays in the form of islands or tilted wires.

3.2 Nonplanar nanostructures *via* vdWE

To address the challenges and limitations in the growth *via* conventional heteroepitaxy, we aim to demonstrate the applicability of vdWE strategy in the growth of nonplanar nanoarchitectures. Therefore, we envisage the following three subobjectives to be accomplished: (1) demonstration of successful nanowire array growth with vdWE; (2) documentation of the characteristics of the vdWE in nanowire array; and (3) extension of the applicability of the vdWE to other nonplanar nanoarchitectures.

3.2.1 The growth of nanowire array. A vertically aligned nanowire array is the simplest construction of nonplanar nanostructures. As vdWE mostly affects only the heterointerface between the epitaxial structure and the substrate, a demonstration of the epitaxy mechanism on a nanowire array is a sufficient proof-of-concept on the applicability of vdWE to nonplanar nanostructures.

Among the earliest attribution of vdWE in a nanowire array is the growth of iron phthalocyanine (α-FePc) "nanobrush" on glass substrate by MBE.[63] Both the nanowire material and the substrate is claimed to be free of unsaturated dangling bonds: FePc is a closed-shell organic molecule while glass is supposedly inert. As the growth product, FePc nanobrushes are oriented perpendicularly from the substrate. However, detailed characterization of the heterointerface of the system was not available. Whether there was a crystalline relationship between the substrate and the nanobrush—which would be needed for categorizing the growth as an epitaxial—is also uncertain since glass is generally amorphous (the substrate was obtained by cutting microscopy slides).

To address the feasibility to apply the vdWE unambiguously, we demonstrated the growth of vertically aligned nanowire arrays grown on a single type of substrate. We used thermal evaporation and vapor transport techniques, which we have also utilized for other 1D nanostructural growth,[64–66] to produce all nanostructures in our studies which are discussed in this article. With the layer-structured muscovite mica as the substrate due to its suitability for vdWE,[35,67] we are able exclusively to grow nanowire arrays from binary semiconductor compounds (Fig. 5; CdS,[35] CdSe,[35,68] CdTe;[35] ZnO,[30] ZnTe,[69,70] and PbS). The possibility of nanowire growth from various compounds on muscovite mica substrate into 3D/2D epitaxy scenario, irrespective of the ensuing lattice mismatch, is in agreement with the characteristics of vdWE. Morphological differences (*e.g.*, size, faceting, tapering, and features) are noticeable from the different nanowires, most probably due to the variation of the response of the different compounds to the kinetics and thermodynamics of the growth as well as a result of the intrinsic crystalline properties from the different compounds.

Each array shares the feature of well-separated nanowires without any buffer/seed layer or intermediate structures connecting the nanowires to the substrate. In the context of the current work, the absence of a buffer layer on epitaxial nanostructure suggests that there is not much strain energy to be released in the system (*i.e.*, the epitaxial structures are already relaxed). The absence of a buffer layer in all compounds cannot be explained in terms of conventional heteroepitaxy as we should expect the presence of a variation in the in-plane lattice parameters—and the inevitable lattice mismatch with the substrate—across the different compounds.[35] We therefore attribute such a strain-relaxed epitaxy to the vdWE mechanism. We remark that well-aligned unbranched ZnTe and PbS array growth is uncommonly reported in literature, which is likely to be due to the difficulty in obtaining suitable substrates for a conventional heteroepitaxial growth. Besides, the strong vertical alignment of the nanowires is also another likely benefit offered by the vdWE on muscovite.[70] For comparison, many of previous reports of nanowire growth *via* conventional heteroepitaxy that require a lattice-matched substrate, *e.g.* ZnTe on GaAs(100),[71] invariably produce a mixture of vertical and tilted nanorods within the same substrate. Therefore, our demonstration of well-aligned nanowire arrays growth without a buffer layer from various materials strongly indicates the success of vdWE in circumventing the requirement of lattice matching.

Beside the growth of pristine semiconductor nanowire arrays on muscovite, we also accomplished the template-free growth of the alloyed CdS_xSe_{1-x} nanowire arrays on a muscovite mica substrate.[72] With the same thermal evaporation and vapor transport synthesis technique, we observed an excellent stoichiometric transfer of the molar ratio of the powder source to the composition of the resulting nanowire arrays. Correspondingly, the lattice parameters of the CdSSe nanowire array can be tuned rationally while adhering to Vegard's law, thus simultaneously allowing the modulation of optical properties. Our work on the growth of the alloyed nanowire arrays thus served a twofold significance. Firstly, we showed a facile growth methodology in producing vertically aligned CdSSe nanowire array with controllable composition modulation. The second and more-intriguing point of the work is apparent when we consider the variation of the cell parameters of the alloy along with the composition. The capability to grow well-oriented nanowires with the variation of cell parameters—and the associated changes in lattice mismatch—validates the application of vdWE in circumventing the lattice mismatch for epitaxial growth.

Other than muscovite mica, there are several layered substrates which have been considered for epitaxial growth of nanowire arrays, although the characteristics of the epitaxy remained unclear. One example is graphene, which has been

intensively studied within the last decade due to its superb material properties.[73] In an earlier example of such studies, Kim *et al.*[74] were able to grow ZnO nanowire arrays on few-layer graphene, conclusively achieving vertically aligned growth in comparison to the randomly oriented growth in SiO_2, which is a bulk substrate and thus necessitates lattice matching conditions for well-aligned epitaxial growth. Kumar *et al.* utilized ZnO nanowire-on-graphene construction to fabricate *in situ* piezoelectric nanogenerators, with the graphene acting as the electrode.[75] However, those studies did not clarify the origin of epitaxial growth and no attribution to the vdWE mechanism. A more recent study by Hong and Fukui did attribute an epitaxial growth of 0.49% lattice-mismatched InAs nanowire array on graphene to the vdWE.[34] However, they argued that the vdWE on graphene is strained coherently, in contrary to the established characteristics of vdWE in thin film structure. They also concluded that mismatch strain prevents the growth of GaAs-on-graphene (−6.22% mismatch) into nanowire array. Although more recently the growth of GaAs nanowire on graphene has been reported by Munshi *et al.*, by recognizing the van der Waals binding of substrate and overlayer, the in-plane lattices at the first-few monolayers of GaAs is still concluded to be strained due to the lattice mismatch.[76] Thus, we view that further detailed studies should be conducted to elucidate the epitaxy in graphene and other layered materials, particularly on whether the vdWE on graphene could also exhibit the expected characteristics of a vdWE growth, such as the incommensurateness and perfect lattice relaxation at the heterointerface (Section 2.6).

3.2.2 Elucidation of vdWE characteristics in nanowire array. In the second step of the demonstration, substantial advances in the understanding of the vdWE mechanism and characteristics in nanowire array at a more fundamental level are needed. We believe that investigation of the epitaxy characteristics of vdWE in nanowire arrays is essential to validate the reliability of the epitaxy strategy in nanostructural growth. In particular, one of the major distinguishing characteristics between van der Waals and conventional heteroepitaxy is the capability of the vdWE to exhibit incommensurateness at the heterointerface. This incommensurate epitaxy allowed the realization of epitaxial growth without any relevance of the lattice mismatch. The presence of this incommensurateness in vdWE was very well characterized in planar structures such as thin films. However, the characteristics of vdWE—whether the incommensurateness exists at all—were not well documented in nonplanar nanostructures.

Using ZnO nanowires on muscovite mica as a model system, we elucidate the characteristics of vdWE in an individual nanowire.[30] Despite the existing lattice mismatch in the system, the nanowires are grown in strong vertical alignment without any apparent buffer layer at their interface with the substrate (Fig. 6a). The hexagonal facets of the ZnO nanowires are also aligned with respect to the substrate (Fig. 6b). The in-plane alignment is as expected in epitaxial growth, due to the presence of an epitaxial crystalline relationship between the substrate and the epitaxial material.[30,31] The epitaxial relation is confirmed by cross-sectional HRTEM observations (Fig. 6c) to be $(0001)[11\bar{2}0]_{ZnO}\|(001)[010]_{mica}$. The absence of a buffer layer and any crystalline defects (*e.g.*, threading dislocations and stacking faults) on ZnO at the heterointerface is interesting, since it suggests that the epitaxial nanowire is not heavily strained. The power spectra (Fig. 6c inset) even showed that the reflection of in-plane lattices of ZnO at the heterointerface is identical to that away from the interface and is not extended to match that from the in-plane lattices of muscovite. These observations are consistent with the characteristics of an incommensurate epitaxy, which we confirmed *via* Fourier filtering of the image at the heterointerface (Fig. 6d). The individual in-plane lattices of ZnO and muscovite are still seen to have different spacing although epitaxial growth has occurred. Moreover, the mismatch at the heterointerface is measured to be −8.26%, close to the theoretical lattice mismatch between bulk ZnO and muscovite. The incommensurate vdWE of ZnO–muscovite is further corroborated by atomic modelling (Fig. 6f). An O-surface termination of the ZnO base is used in the modelling, as justified from the polarity of the nanowire determined *via* aberration corrected

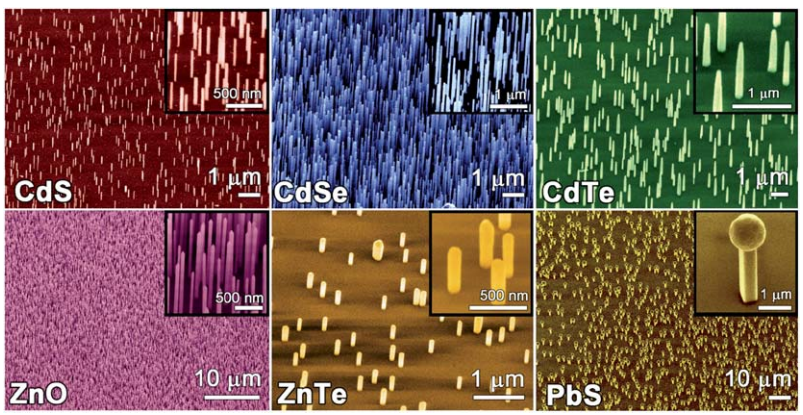

Fig. 5 Morphological characterizations of the as-synthesized arrays grown on muscovite mica substrate. All of the nanowire arrays were grown in a catalyst-free synthesis. The SEM images of the as-grown nanowire arrays from various compounds were recorded in 45° tilted view. The insets show SEM images of the sample at higher magnification. All of the micrographs were pseudocolored.

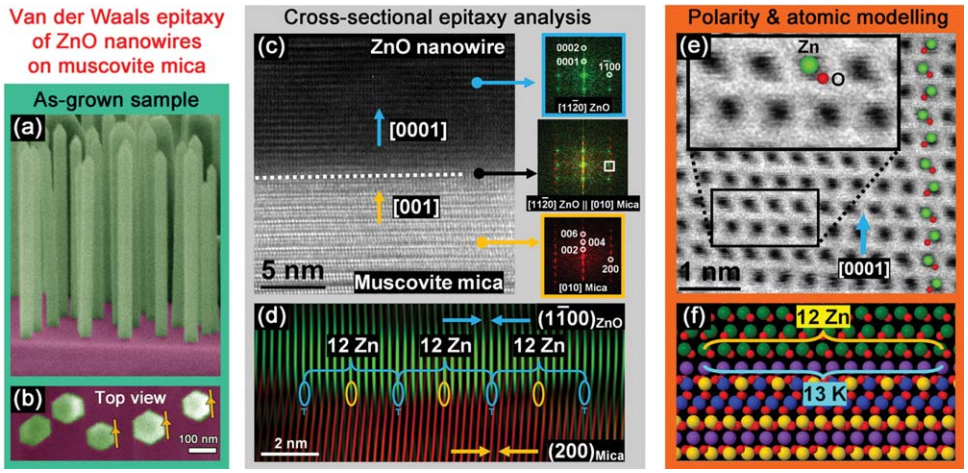

Fig. 6 Characterization of a van der Waals epitaxial nanowire array, with ZnO-on-muscovite as a model system. (a) Cross-sectional SEM image of the as-grown sample. (b) Top view SEM image, showing the in-plane facet alignment of neighbouring nanowires. (c) Cross-sectional HRTEM image of the heterointerface in the $[11\bar{2}0]_{ZnO}||[010]_{mica}$ zone axis. Inset: power spectra of (upper, pseudo-colored in red) ZnO nanowire, (lower, in green) muscovite mica substrate, and (middle, color-combined) the nanowire–substrate interface. (d) Fourier-filtering of the image in (c), showing only planes normal to the zone axis which form the vector alignment in the epitaxy *i.e.*, $(1\bar{1}00)_{ZnO}$ and $(200)_{mica}$. (e) ABF-image of ZnO nanowire, with a blue arrow denoting the growth direction of the nanowire. The Zn–O atomic dumbbells are superimposed with green (red) balls for Zn(O) atoms to clarify the orientation and the wurtzite ABABAB stacking. Inset: zoom-in of the region marked with black rectangle. (f) Atomic modelling of the epitaxy, showing the matching of $(1\bar{1}00)_{ZnO}$ and $(200)_{mica}$ planes. (Adapted from ref. 30 with permission.)

annular bright field scanning transmission electron microscopy (ABF-STEM) (Fig. 6e).[77]

We believe that the characteristics of vdWE established for ZnO nanowires should also applicable for other nanowire array materials as well. The cross-sectional HRTEM analysis of ZnO—as a representative of the compounds that have been grown as nanowire arrays on mica (*e.g.*, Fig. 5)—is already sufficient for the main purpose of our current study, which is the investigation of the epitaxy characteristics of nanowires (and nonplanar nanoarchitectures in general). We have shown that the vdWE is actually incommensurate. Thus, any parameters regarding the crystallinity of the nanowire material, including their phase and lattice constants, are irrelevant for the vdWE to occur. Besides, the vdWE is also expected not to involve chemical bonding between the epitaxial material and the substrate,[11] making the chemistry of the epitaxial material an irrelevant issue as well.

3.2.3 Generalization of the vdWE to nonplanar polytypic nanostructures. To establish the general applicability of van der Waals on nonplanar nanostructures, we demonstrated that vdWE can be extended for epitaxial growth in other morphologies as well. We then focused our effort on the growth of branched semiconductor crystals, comprising tripods and tetrapods (Fig. 7).

With vdWE on the muscovite substrate, we reported the growth of tripod crystals in epitaxial form.[31] As vdWE does not require lattice matching, the structure—possessing three symmetrically branched legs—could be grown epitaxially from various II–VI semiconductor compounds. As a manifestation of the epitaxy to the mica substrate, the legs of adjacent tripods within the same substrate are aligned in only two possible in-plane orientations. We exemplify such an in-plane alignment in Fig. 8, with the two orientations being anti-parallel to each other and related by a 60° rotation. Similar in-plane leg alignments in only two orientations were also observed in van der Waals epitaxial tetrapods, whose synthesis was first reported in ZnTe.[70]

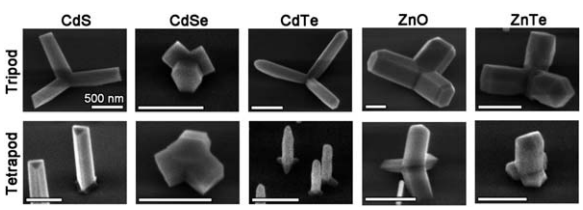

Fig. 7 Selection of SEM images of nonplanar semiconductor nanostructures grown on muscovite mica *via* vdWE: tripods, and tetrapods. All scale bars: 500 nm. (Adapted from ref. 31 and 70 with permission.)

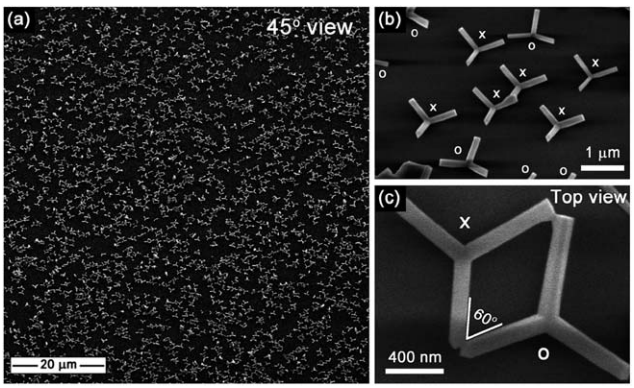

Fig. 8 In-plane alignment in van der Waals epitaxial CdS tripods. (a and b) The SEM images of the tripods in 45° tilted view in low and high magnification, respectively. The two in-plane orientations of the legs are marked with "o" and "x" in (b). (c) Top view SEM of neighboring tripods in the two possible orientations, showing that the orientations are related by a 60° rotation. (Adapted from ref. 31.)

Since then, we have also been able to increase the number of compounds where epitaxial tetrapods could be produced, encompassing other members of II–VI semiconductors as well, as reported here for the first time (Fig. 7, lower row). The growth of the tripods and tetrapods are thus in accordance with the characteristics of the vdWE, thus effectively demonstrating the universal capability of vdWE for nonplanar nanoarchitectures.

We now discuss the results of the morphological and structural characterizations of the structures. Fig. 7 illustrates the resemblance between the morphology (*e.g.*, cross-sectional shape, faceting at the tip, and size scale) of the legs of epitaxial tripods and tetrapods to that of vertically aligned nanowires of the same compound, all of which were grown on the muscovite mica substrate *via* vdWE. The similar morphology between the legs of branched crystals and the vertical nanowires suggests that they might share similar crystallinity and polarity as well. For instance, the ZnO nanowires are grown in the wurtzite (WZ) phase with growth direction along the positive *c*-axis $[0001]_{WZ}$, as corroborated with HRTEM and ABF-STEM.[30] The overall faceting of the ZnO structure, including the hexagonal cross section and truncated hexagonal pyramidal taper, is in agreement with the idealized crystal habit of WZ ZnO grown along $[0001]_{WZ}$ (*i.e.*, the positive *c*-axis).[78] Hence, due to the similarity between ZnO nanowires and tripod legs, we can hypothesize that the legs of ZnO tripods were grown along $[0001]_{WZ}$ as well.

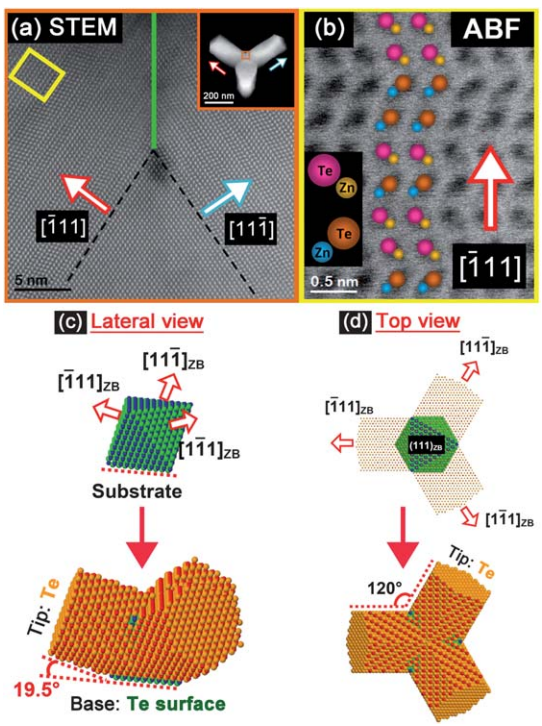

Fig. 9 Characterization and modelling of ZnTe tripods. (a) STEM of the junction area of a tripod, at the region as indicated with a brown square in the inset image. The green line marks the location of a twin boundary. (b) High magnification ABF-STEM image in the region as marked with yellow rectangle in (a). Atomic modelling was constructed on the growth mechanism of the tripod in (c) lateral view and (d) top view, where the growth mechanism from a {111} octahedra seed is assumed. (Adapted from ref. 70.)

Characterizations on epitaxial ZnO, CdS[31] and ZnTe[70] tripods, as a representative of branched crystals, showed that the tripods have a polytypic structure with legs in the hexagonal wurtzite (WZ) phase and a junction in the cubic zincblende (ZB) phase (*e.g.*, Fig. 9a and b). Regarding the structure of the tripods, we observed: 120° angle separation of the legs measured from top view (Fig. 8c and 9e); ~19.5° upward-inclination of legs from the substrate;[31] and ~111° angular separation of adjacent legs that are separated by a twin (see Fig. 9b). Such a tripod structure is consistent with crystals following seeded growth mechanism of WZ legs on an octahedral ZB seed, similar to the model proposed by Shiojiri and Kaito.[79] According to the model, the growth of WZ legs along the *c*-axis is introduced by stacking faults only along the $\{111\}_{ZB}$ facets of the octahedral seed with the same polarity to the preferred growth polarity of the legs. In ZnTe, with legs growing along the Te polarization, three legs can grow on three Te-terminated $-\{111\}_{ZB}$ facets of the octahedral seed in an upward inclination from the substrate if the seed has one remaining Te-terminated facet that can be heterointerfaced epitaxially to the substrate (Fig. 9d). The seeded growth mechanism for the growth of 3D nanostructures was also reported in heteroepitaxy recently.[80,81] The long-standing idea of the importance of polarity conservation in the growth of branched crystals was confirmed *via* HAADF- and ABF-STEM observation of atomic dumbbells at ZnTe tripod legs (Fig. 9c); the polarity of crystal along the growth direction of the legs of the tripod and that of the nanowire are identical.[70] This result in turn strengthens the hypothesis that the resemblance in crystal shape and habit between the nanowires and legs of branched crystals implies identical crystal phase and polarity between the two structures.

According to the characterization results on nanorods, tripods, and tetrapods, there are aspects of crystal growth that could strongly influence the resulting products of vdWE. Namely, the growth environment of the structure could be adjusted in order to exploit twinning, polytypism, and polarity in modulating the morphology of the nonplanar van der Waals epitaxial structures.[70] vdWE plays an important role as it allows epitaxial growth of the lattice-mismatched structure and it allows a different crystal polarity to be interfaced onto a polar substrate (*e.g.*, ZnTe nanorods have a Zn^{2+}-terminated base, whereas tripods have a Te^{2-}-terminated base; both are grown on the K^{+}-terminated surface of muscovite mica).[70] In contrast, substrates with a polar surface in most cases of conventional heteroepitaxy dictate the polarity of the epitaxial material at the heterointerface.[82] Thus, it is uncommon to have material that grows into both epitaxial nanowire arrays and tripods in the same polar substrate, except if the material is capable of bidirectional growth (*e.g.*, InP where [111]A and [111]B growth directions are both attainable, depending on the dopant).[81]

4 Synthesis control and growth mechanism of nanowire arrays in vapor-based vdWE

Due to the different nature of the epitaxy mechanism, it is reasonable to examine whether epitaxial nanostructures grown in vdWE could achieve the same level of controllability and

predictability to those produced *via* conventional heteroepitaxy. Here we address the growth mechanisms of ZnO nanowire arrays grown on a muscovite mica substrate,[30] as an example of growth aspects of nonplanar nanostructures in van der Waals epitaxy from vapor-based synthesis. While the following discussion is applicable for ZnO nanowires, it is not necessarily suitable for other compounds and structures due to the difference in chemistry and the kinetics-thermodynamics interplay during the growth, despite being produced from an identical growth protocol.

Metal-rich particles, which are commonly found in conventional vapor–liquid–solid (VLS) growth,[83] were not observed from both the tip and the base of the nanowires (Fig. 10). Considering the catalyst-free nature of our synthesis method, we hypothesize that the ZnO nanowires are growing by a vapor–solid (VS) mechanism, with the anisotropic growth dictated by the growth kinetics of ZnO crystal facets.[78]

To evaluate the growth mechanism of the ZnO nanowire array, we consider our observation of hexagonal ZnO nanoflakes on the samples (Fig. 11). We occasionally discovered that flakes (also commonly referred to as plates, platelets, or sheets in the literature) with a hexagonal shape were interspersed alongside the ZnO nanowire arrays on the muscovite mica substrate. The nanoflakes were typically of the same cross-sectional size as the nanowires, albeit with a much smaller aspect ratio (Fig. 11a). HAADF-STEM results further verified the hexagonal cross-section (Fig. 11b, left). Atomic resolution imaging showed that such a structure is highly crystalline (Fig. 11b, right), where the diffraction pattern from the FFT of the image showed that the structure is in the wurtzite crystal phase with faceting identical to that of ZnO nanowires (Fig. 11b, inset). EDX analysis (Fig. 11c) showed that the flakes are ZnO with an homogenous distribution of Zn and O, except at the broken region on the left side which can be attributed to imperfect separation from the mica substrate. Considering that the hexagonal flakes followed an in-plane orientation ordering relative to the substrate (Fig. 11a), the good crystallization strongly suggests that the structure was also grown by vdWE to the substrate. Hence, due to the substantial resemblance of the ZnO nanoflakes to nanowires in terms of their crystalline phase, faceting, and composition, we strongly believe that such nanoflakes are a

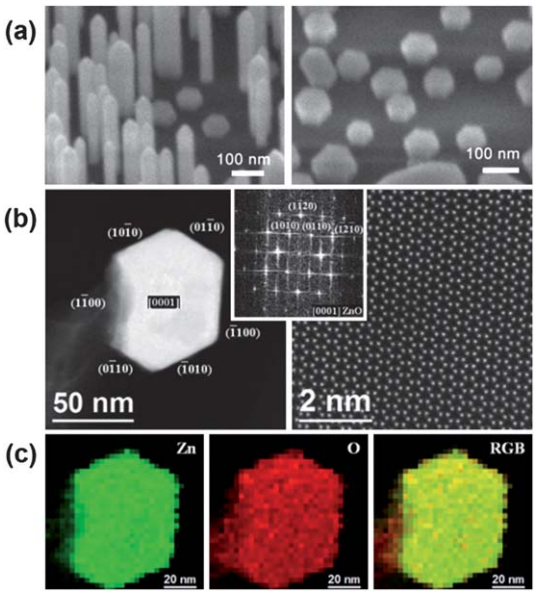

Fig. 11 Hexagonal ZnO nanoflakes found in a sample grown at 750 °C. (a) SEM of the flakes, which can be found interspersed alongside the nanowire array on the mica substrate. (b) Aberration-corrected HAADF-STEM of the hexagonal flakes in low magnification (left) and high magnification (right). Inset: FFT of the high magnification HAADF-STEM image. (c) EDX analysis, showing the areal density of Zn (upper left, color-coded in green) and O (upper middle, in red). Compositional mapping of the hexagonal flakes, taking into account the Zn and O edges, is shown in the right column.

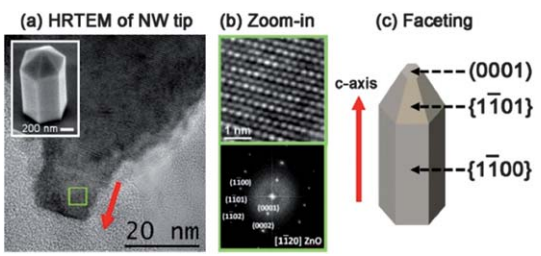

Fig. 10 ZnO nanowire tip and faceting. (a) HRTEM of nanowire tip, of typical sample morphology as shown in SEM at the inset. (b) Zoom-in (upper) and power spectrum (lower) of the region marked with a green square in (a). (c) Taking into account the positive *c*-axis growth direction as deduced from the polarity determination, the faceting of the nanowires is consistent with the idealized growth habit of ZnO.

"seed" (*i.e.*, an initial stage) of the nanowire array growth prior to the axial elongation.

We then discuss the plausibility of commonly ascribed mechanisms of nanowire growth to our experimental data. In the synthesis of a nanowire, a principal requirement for a growth mechanism is to rationalize the anisotropic growth of the structure, *i.e.*, to examine the origin of the growth disparity in the axial and lateral/radial direction. In our present study, no foreign metallic species, such as gold colloidal particles or films, were introduced to the substrate prior to the synthesis. Additionally, no spherical particles are found at either end of the nanowires. Therefore, we can neglect the possibility of conventional VLS growth in our system.

Several mechanisms have been proposed for the growth of catalyst-free vapor-based synthesis of ZnO nanowires, including: (a) dislocation-driven mechanism;[84,85] (b) self-catalytic;[86] and (c) VS growth.[87] In the dislocation-driven mechanism, the growth of nanowires are seeded by a dislocation, which promotes the anisotropic growth of nanowires by the propagation of spiraling screw dislocations along the nanowire axis. However, all ZnO nanowires that we have observed were free from axial dislocation; as such the dislocation-driven mechanism might be unlikely. The self-catalytic mechanism utilizes a catalyst which is composed of elements that also constitutes the material of the nanowires, *e.g.*, a Zn catalyst for the growth of ZnO nanowires. However, there are three major experimental observations that conflict with the self-catalytic mechanism. Firstly, the hexagonal nanoflake seeds are ZnO in composition, with uniformly distributed Zn and O constituents

(Fig. 11c). Self-catalytic growth requires Zn-rich sites to be consumed for the anisotropic axial elongation, such that the seed should have contained a high Zn concentration if we assume the self-catalytic growth to be relevant. Secondly, the self-catalytic mechanism fails to explain the behaviour of the growth at the tip of nanowires. The well-faceted pyramidal tip of nanowires (*c.f.*, Fig. 10c) disagrees with past reports on self-catalytic nanowires where the tip is usually more rounded[86,88] due to the shrinkage of the catalyst which is thought to be in liquid droplet form. The protrusion emerging at the tip (Fig. 10a) also strongly suggests that no catalyst droplet is necessary during the growth process, as a Zn-rich site cannot be found by both EELS and EDX mapping. Therefore, we conclude that the self-catalytic mechanism cannot be solely responsible for the growth of ZnO nanowire arrays with our method, although the mechanism might have contributed to the growth process in the very early stages when Zn species still existed on the substrate.

The VS mechanism is a process where the vapor reactant spontaneously condenses into the solid phase, thus requiring no catalyst during the growth.[89,90] Similar to the case of heteronucleation of a thin film on a solid substrate with the vapor deposition technique,[4] the driving force for nucleation in the VS growth mechanism is the supersaturation of the ambient vapor phase. Anisotropic growth of the crystal into the nanowire structure is dictated by the relative growth rate of the different crystal planes of the material.[91] Indeed, the faceting and morphology of the ZnO nanowires (Fig. 10) is in strong agreement with the idealized growth habit of the ZnO crystal which has a (0001) Zn-terminated surface as the fastest growth front.[78,92] Self-limiting growth can therefore be attributed to the formation of pyramidal tapering, which inhibits further axial elongation when the top (0001) surface disappeared completely. Additionally, in the context of VS growth, a narrow diameter distribution is also attributable to the supersaturation-controlled critical nucleus size,[93] showing that the phenomenon is not unique only to the VLS mechanism. On the other hand, the length–diameter correlation is also a consequence of further growth of the well-faceted pyramidal tip, which is composed by $\{1\bar{1}01\}$ side facets, when the base of the pyramid is larger in larger diameter wires. Hence, as compared to other mechanisms as discussed previously, VS growth is the most feasible mechanism in explaining many aspects of the ZnO nanowire growth on muscovite mica.

Fig. 12 shows the schematic of the growth that may occur in our synthesis of ZnO nanowire array. After the evaporation of ZnO *via* hydrogen-assisted thermal decomposition as given in reaction shown within the Figure, the vapors are transported onto the substrate which is positioned in the lower temperature region of the furnace. Although the vaporized Zn may react with the gaseous H_2O (*i.e.*, water vapor) to return to ZnO, the Zn species may also deposit onto the substrate directly. Thus, it is very likely that the Zn adatoms become the preferential adsorption sites, similar to their role in the self-catalytic mechanism. Continual oxidation of the Zn sites by the inlet of water vapor eventually causes supersaturation, followed by heteronucleation and crystal growth in nanoflakes by vdWE. However, absence of Zn-rich sites at the end product of ZnO of both nanoflakes and nanowires suggests that the oxidation fully transforms the Zn-rich sites into ZnO crystals before the completion of nanoflake growth. Next, the VS growth mode proceeds to produce vertically aligned nanowires, as the highest growth rate is along the positive *c*-axis.

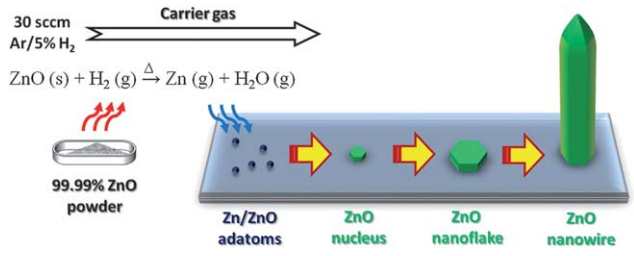

Fig. 12 Schematic of the synthesis and growth process (not to scale).

5 Optical characterizations of as-grown vdWE nanowire arrays on muscovite

In previous sections, we have established that vdWE has comparable ability with the conventional heteroepitaxy in producing nanostructured samples of good crystalline quality. To strengthen our point that nanostructures from vdWE are equivalent to those from conventional epitaxy, we performed steady-state optical characterizations on ZnO and CdSe nanowire array samples from vdWE, including both photoluminescence and Raman spectroscopy. Steady-state photoluminescence spectroscopy can probe the electronic band structures and identify the excitonic states.[68,94] On the other hand, Raman scattering spectroscopy has been shown as a powerful technique to investigate crystalline phase purity,[31] surface modulation leading to activation of surface optical phonon scattering,[95,96] phonon confinement[97,98] and the optical antenna effect due to quantum size and strong anisotropy,[96,99,100] or phonon–plasmon interactions.[101,102] Our results exemplify that nanostructures from vdWE are of excellent optical grade material befitting applications and further studies. Hopefully, these optical studies further stimulate in-depth investigations of vdWE synthesis of nanostructures and heterostructures and their optical and optoelectronic properties.

For both room temperature and low temperature micro-Raman and micro-photoluminescence (PL) spectroscopy, the ZnO and CdSe samples are pasted onto glass cover-slips and attached in a liquid nitrogen continuous flow cryostat (Cryo Industry of America). UV-vis spectroscopy is performed with a spectrometer (PerkinElmer Lambda 950). Micro-Raman and micro-PL spectroscopy were both performed with a micro-Raman spectrometer (Horiba-JY T64000) in a backscattering geometry. For micro-Raman spectroscopy, the ZnO and CdSe samples are both excited by a focused beam of 532 nm laser. For micro-PL, 355 nm (ZnO) and 532 nm (CdSe) laser excitations were used. The back-scattered signal was collected by the same objective and dispersed by 1800 g mm^{-1} grating in single mode with a spectral resolution of $\sim$1 cm^{-1}, and recorded by a liquid nitrogen-cooled charge coupled device detector. Micro-Raman

spectroscopy was performed on individual nanowires; the as-grown sample is ultrasonicated and drop-casted on an indium foil. The amplified spontaneous emission in ZnO was demonstrated by optical pumping from a pulsed Nd:YAG 355 nm laser (repetition rate: 10 Hz, pulse duration: 5 ns), which was focused by a UV objective (×40, NA: 0.4) before the excitation on the sample at 120 K.

Fig. 13 shows the optical characterizations that we conducted on ZnO nanowire array grown from vdWE similar to that shown in Fig. 5. The measured Raman shift of those phonon modes and their assignments are given in the graph. Generally, the features are very similar to what was found in bulk ZnO samples:[103,104] the intense and sharp peaks at 98.9 and 437.4 cm^{-1} are generally assigned to the two modes from E_2 phonons. The band at 331.4 cm^{-1} was previously considered to be non-fundamental and assigned as a multi-phonon, second-order mode. More recent work suggested that this mode is actually a process involving the difference of the lower and higher frequency E_2 modes.[105] Transverse-optical (TO) modes with A_1 and E_1 symmetries are observed, whose position matches well with that reported in literature. However, our sample differed in that we did not observe the longitudinal-optical (LO) modes of A_1 and E_1 which are supposed to be located at 583 and 574 cm^{-1}, respectively, for the bulk sample. The absence of LO phonons, however, was also reported for ZnO nanobelts.[106] Meanwhile, the assignment of an additional broad feature centered at 553.0 cm^{-1} is rather controversial; there is no consensus from previous works as the peak has been attributed to surface phonons from (1–100) facets,[107] to oxygen deficiency,[108] and also to multiphonon processes.[103]

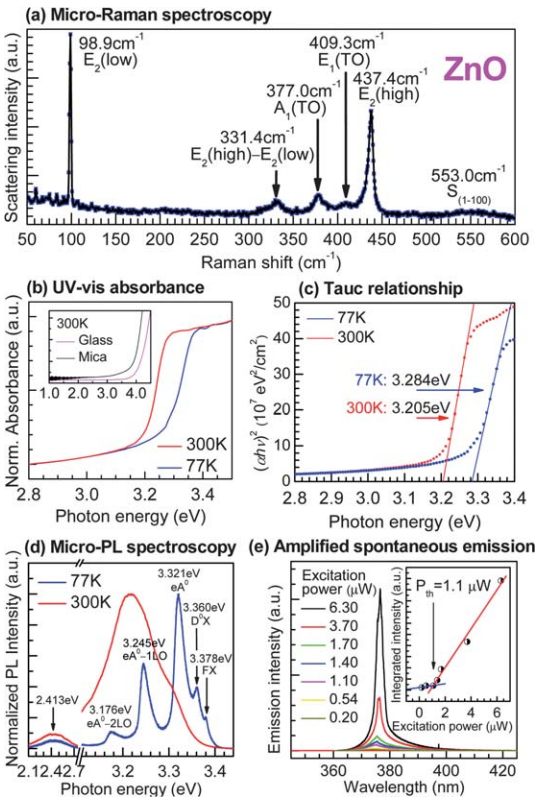

Fig. 13 Optical characterizations on van der Waals epitaxial ZnO nanowire array.

Both muscovite and glass are highly transparent under optical light below <3.5 eV (see inset Fig. 13b), aside from a small oscillation on muscovite under the infrared regime (1–2 eV) which is ascribable to interference of the probe light due to the layered nature of the substrate.[35] The transparency allows the usage of muscovite for *in situ* optical characterization. A sharp absorption edge of ZnO at 300 K is noted at around 3.2 eV (Fig. 13b), close to the expected bandgap of bulk ZnO. The blueshift of the feature when the temperature is decreased to 77 K corroborates the relation to near band-edge absorption; the bandgap typically increases with decreasing temperature due to the shrinkage of the crystal lattice and modification by electron–phonon interaction.[68] The value of the bandgap is determined from Tauc's relationship: $\alpha h\nu \propto (h\nu - E_g)^{1/2}$, where α, $h\nu$, and E_g are the absorption coefficient, photon energy, and the optical bandgap, respectively.[109] As is demonstrated in Fig. 13c, the equation implies that the *x*-intercept from linear fits of $(\alpha h\nu)^2$ *versus* $h\nu$ is the electronic bandgap of the sample. The room temperature ZnO bandgap of 3.20 eV is well within the commonly reported bandgap values of ZnO bulk single crystals (3.1–3.3 eV).[110] The absence of quantum confinement-related blueshift was as expected considering that the nanowire diameter (Fig. 11) is still larger than the exciton Bohr radius of ZnO (~2.34 nm).[111]

Aside from the strong near-bandedge emission (~3.2 eV) which agrees with the UV-vis data, the room temperature PL spectrum of ZnO (Fig. 13d) only exhibited a much weaker green emission at 2.4 eV (~514 nm). The green emission has been attributed to the presence of deep-level intrinsic defects such as oxygen vacancies[112] and anti-sites;[113] the relative weakness of the green emission showcases the good quality of the nanowire. Various spectral features emerged at low temperature (77 K); the peak positions and assignments in Fig. 13d are in agreement with results presented in both the bulk[114] and in nanorods.[115] Although free exciton emission (FX) is recognizable, the spectrum is dominated by transition of free electrons to neutral acceptor (eA^0) and by neutral donor-bound exciton emission (D^0X). Two LO phonon replicas of eA^0 accompanied the main excitonic emissions with energy separations of 76 and 70 meV, comparable to the expected energy of LO phonons (72 meV).[114]

The intensity of the emission increases as the excitation power is increased, as shown in Fig. 13e for excitation in the range of 0.20 μW to 6.30 μW at 120 K temperature. As shown in the inset of Fig. 13e, the integrated intensity of the emission is linearly proportional to the excitation power. However, the slope of the straight line fit changes dramatically at ~1.1 μW. Additionally, there is a reduction of full-width at half maximum from 74.3 meV (@0.20 μW) to 24.9 meV (@6.30 μW). These results are consistent with the occurrence of amplified spontaneous emission[116] with an excitation power threshold (P_{th}) of ~1.1 μW. The emission appeared as only a single peak instead of regularly spaced modes even after the power exceeded P_{th}. Thus, verification of lasing action with the nanowire length as the resonance cavity—as was previously reported with a ZnO nanolaser[57]—cannot be performed in our sample.

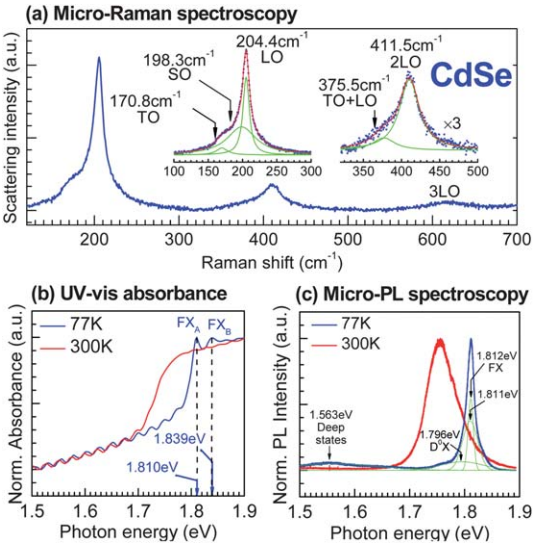

Fig. 14 Optical characterizations on the van der Waals epitaxial CdSe nanowire array.

A similar set of optical characterizations were also performed on the CdSe nanowire array with vdWE. For the micro-Raman spectrum of CdSe, the peak positions are in strong agreement to those reported in a CdSe nanobelt structure by Venugopal *et al.*,[117] which in turn were in agreement with that of the bulk structure.[118–120] The assignment of the Raman peaks according to previous studies is given in Fig. 14a. For the UV-vis absorption spectra at room and low temperatures (Fig. 14b), oscillation of the spectra can be noted for energies below 1.8 eV. The origin of the oscillation is similar to that shown in the inset of Fig. 14b: interference due to the layered structure of the substrate.[35] For absorption spectra at low temperature, two additional peaks emerged at 1.810 and 1.839 eV. These peaks are assigned to the free-exciton A and B emissions, respectively.[121,122] Coincidentally, the energy of FX_B is very close to that of the phonon replica of FX_A (FX_A-1LO);[68] more investigation is needed to clarify the nature of the peak.

Similar to the luminescent property of van der Waals epitaxial ZnO nanowires, the CdSe nanowires exhibited strong near band-edge emission (Fig. 14c). Only a weak and broad deep defect emission is spotted at ~1.5 eV.[123] The fitting of the near band-edge emissions reveals three features: (1) a broad shoulder centered at ~1.80 eV which can be attributed to neutral donor-bound excitons;[120] (2) a sharp peak at 1.812 eV which is attributable to free exciton emission; (3) and a slightly weaker and broader peak than (2) at a similar location, which may be due to excitonic interactions. A detailed discussions on the excitonic properties of van der Waals epitaxial CdSe nanowire array and a demonstration of near-infrared random lasing from the structure have been published elsewhere.[68]

6 Recent progress and perspective for future research directions on vdWE

The fundamental advances on the understanding and applicability of vdWE as described herewith in this article might contribute to opening various avenues of future research directions. With regards to existing works on vdWE in the literature, future directions of studies that should be pursued relative to the current state of research on vdWE may be divided into two categories: (1) future studies aiming to develop and improve the vdWE as a methodology for materials preparation; and (2) future studies exploiting epitaxial materials as the result of the unique characteristics of vdWE. We shall discuss only the former category, given that the latter ones are too diverse to be discussed within this article. Thus, this section highlights several possible studies that may be conducted in order to improve the capability of vdWE and to gain a comprehensive understanding of the vdWE phenomenon, toward its actualization and real world impact in technological applications.

6.1 Other materials, substrates, and architectures

As one of the characteristics of vdWE, lattice matching is not crucial for achieving well-crystallized epitaxial growth. Thus, we expect that the range of materials that could be prepared epitaxially into nonplanar nanoarchitectures with the vdWE mechanism could be expanded to various other classes of materials, not limited only to II–VI, III–V, and IV–VI binary semiconductor compounds. Emphasis may be given to intensively researched compounds with strong prospective applications, such as TiO_2 for photocatalysis[124] and iron pyrite for photovoltaics,[125] and compounds that have previously been uncommon in the epitaxial form.

We also expect that vdWE will be applicable for the growth of other epitaxial nanostructures on various substrates that satisfy the requirements of a weakly reactive surface. Future works in this direction will have significant impact by not only demonstrating the generality of the vdWE, but also by opening new possibilities for device fabrication when the substrate also has exotic and utilizable material properties. Layered materials are of particular interest to be used as van der Waals epitaxial substrates, due to the wealth of material properties that can be accessed and coupled with those from the grown epitaxial nanostructures for device applications. Varieties of electronic properties from layered materials have been well documented,[12] ranging from insulating (such as phlogopite, zeolite, and the rest of mica class), semiconducting (MoS_2, $MoSe_2$, WS_2, WSe_2, TiS_2, BN), metallic ($TaSe_2$, NbS_2, WTe_2), semimetallic ($TiSe_2$), superconducting (TaS_2, $NbSe_2$), to topological insulating[126,127] (Bi_2Se_3, Bi_2Te_3). Thus, those layered materials may be used in a suitable role for electronic and optoelectronic applications based on materials produced by vdWE. For example, conducting layered materials may be used as both the substrate and the electrical contact in devices from as-grown materials. Relevant to the utilization of those layered materials as the substrate for vdWE, it is also interesting to study the behavior of the epitaxial system when the substrate is atomically thin, down to the single to few-layer level only, in which the substrate exhibited 2-dimensionality. With vdWE, small-diameter nanowire arrays can be grown on such 2D substrates to form hybrid quasi-1D/2D systems, for which the arising novel properties from the materials might be exploited for innovative devices. Another way to

expand the applicability of the vdWE is to perform the growth of nonplanar epitaxial nanoarchitectures with higher morphological and crystalline complexity. For example, we believe that our vdWE demonstration in nanowire arrays and epitaxial tripods could be extended for the growth of hierarchical nanostructures,[128,129] and heterostructures (both radial/core–shell[130,131] and axial[132]).

It is logically reasonable to expect that the vdWE may be extended to other nanoarchitectures and compounds. We showed that the vdWE is applicable to the growth of well-crystallized nanowire arrays from various compounds without regard to lattice mismatch.[30,31,35] These compounds even show variation of their crystalline phases (ZnO, CdS, CdSe: hexagonal; ZnTe, CdTe: cubic; PbS: rocksalt)[35,133] that are dissimilar to the crystalline symmetry of the surface of mica, which has a monoclinic phase. We then attribute the incommensurateness of the heterointerface as the reason for the possible epitaxial growth from many different compounds with various crystalline phases and lattice constants, which otherwise would not be feasible in the case of conventional heteroepitaxy. With such an incommensurateness, we view that it is conceivable that other compounds with other crystalline phase and cell parameters could also be grown. Once the epitaxial growth is achieved, we believe that it is of secondary difficulty to attain a more complex nanoarchitecture. For example, extra growth steps could be performed in order to nucleate branches into the nanowires—now serving as the backbone—to achieve a hierarchical structure. vdWE relaxes the strict requirements of the overlayer–substrate crystalline relationship and is thus superior to conventional heteroepitaxy. Therefore, the vdWE should also be effective in growing other crystalline structures that can be prepared *via* conventional heteroepitaxy, with the exception for structures occurring because of excessive strain (*e.g.*, the defect-rich buffer layer).

6.2 van der Waals epitaxial growth in solution-based synthesis

With the exception of the work by Zasadzinski *et al.* on Langmuir–Blodgett films,[134] most of the material growth invoking vdWE had been performed using a vapor-based synthesis approach. It is therefore reasonable to question whether solution-based syntheses are also capable of producing nonplanar epitaxial material by vdWE. The ability to accomplish van der Waals epitaxial growth in different synthesis routes will also support the promising future of vdWE as a universal epitaxy strategy.

One current effort pursued in our group is to investigate whether the vdWE of a nanowire array could also be achieved in hydrothermal synthesis. Hydrothermal synthesis is a form of solution synthesis with water as the solvent. This synthesis route has been demonstrated in the growth of a ZnO nanowire array[135] and is now very well established in producing nanostructures from a variety of materials. The hydrothermal synthesis has a major benefit when compared to other vapor-based synthesis: the growth can be conducted at low temperature (<100 °C) and able to produce nanostructures with good uniformity covering a wide area of the substrate, even reaching wafer-scale growth.[136]

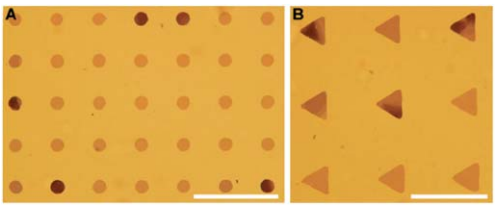

Fig. 15 Optical micrograph of (a) round and (b) triangular Bi_2Se_3 nanoplate array on mica. The ordering is achieved by lithography. Scale bars: 100 μm. (Adapted from ref. 24.)

Further works are necessary to completely understand various aspects of the hydrothermal vdWE, including how the chemistry of the substrate surface would be affected by the solution, the extent of the stability of the substrate with the growth environment, and on the growth mechanism of the epitaxial nanostructures. Besides, careful adjustments of the growth parameters are needed to optimize the morphology and crystallinity of the as-grown nanowire arrays. Our results on this effort will be reported elsewhere.

6.3 Control of positioning *via* lithography

Positioning control is an issue that needs to be addressed in every fabrication technology for the reliable and repeatable production of devices based on nanostructures.[137,138] There are numerous methodologies to allow the growth of nanostructures into ordered arrays, such as by using lithography method to pattern area for which the nonplanar nanoarchitectures are to be grown. A recent study by Li *et al.* utilizes a combination of UV photolithography/copper masking and oxygen plasma etching to modify selectively the surface of the mica substrate.[24] Consequently, the synthesis of Bi_2Se_3 and Bi_2Te_3 nanoplates could be performed by vdWE while achieving position- and orientation-control (Fig. 15).

It is also interesting to extend the effort of lithography in vdWE for nonplanar nanostructures. However, given the limited lateral size of nanostructures, lithography techniques with a better resolution capability are needed. One lithography method that is prospective in our nanostructures-on-mica system is laser interference lithography. The laser interference lithography has been shown previously to allow positioning control in a ZnO nanowire array,[139] even reaching wafer scale growth in a recent study.[140] Laser interference lithography is expected to be suitable for our epitaxial samples on muscovite mica because, unlike e-beam lithography, the lithography method does not necessitate a conducting substrate. However, the question of whether our catalyst-free growth method allows the growth of nanowire array on the exposed area of the substrate (*i.e.*, patterned positions which are uncovered by any resist or dielectric) remains to be addressed.

Conclusions

We have demonstrated the application of vdWE for the growth of nonplanar nanostructures (nanowires, tripods, and tetrapods) from various semiconductor compounds using only a

single type of substrate—namely, muscovite mica. Good crystallization during the epitaxial growth was accomplished despite the variation of in-plane lattice parameters in each compound, and we should thus expect that there will be a wide range of lattice mismatch values between the different nanostructures and the mica substrate. Our characterization results on nanowire arrays showed that the in-plane lattices of the nanowire and the substrate at the heterointerface are incommensurate. The possibility to achieve an incommensurate epitaxy with the vdWE is one of the major reasons for the successful growth of nanowire arrays from various compounds on mica substrates regardless of their lattice mismatch.

The most fascinating advantage of the vdWE over conventional heteroepitaxy is the possibility to achieve epitaxial growth without the strict requirements of lattice matching. As such, vdWE allows the growth of epitaxial structures from various compounds irrespective of their lattice mismatch to the substrate suitable for vdWE. Such a feature could have widespread consequences and immediate applications, providing richer opportunities of fundamental studies and technological applications with the use of vdWE.

Acknowledgements

Q. X. acknowledges the strong support from the Singapore National Research Foundation *via* a fellowship grant (NRF-RF2009-06), Singapore Ministry of Education *via* two Tier 2 grants (MOE2011-T2-2-051 and MOE2012-T2-2-086), generous start-up grant support (M58110061) and the New Initiative Fund (M58110100) from Nanyang Technological University. J. A. and F. J. B. acknowledge the funding from the Spanish MICINN projects MAT2010-15138 (COPEON) and CSD2009-00013 (IMAGINE) and Generalitat de Catalunya (2009 SGR 770 and NanoAraCat). The authors thank the TEM facilities at the Universitat de Barcelona and INA-LMA at University of Zaragoza.

Notes and references

1 A. Koma, K. Sunouchi and T. Miyajima, *Microelectron. Eng.*, 1984, **2**, 129–136.
2 J. E. Ayers, *Heteroepitaxy of Semiconductors: Theory, Growth, and Characterization*, CRC Press, Boca Raton, FL, 2007.
3 A. Koma, K. Sunouchi and T. Miyajima, *J. Vac. Sci. Technol., B*, 1985, **3**, 724.
4 H. Lüth, *Solid Surfaces, Interfaces and Thin Films*, Springer, Berlin, Heidelberg, 4th edn, 2001.
5 K. Takayanagi, Y. Tanishiro, S. Takahashi and M. Takahashi, *Surf. Sci.*, 1985, **164**, 367–392.
6 J. Narayan and B. C. Larson, *J. Appl. Phys.*, 2003, **93**, 278–285.
7 F. C. Frank and J. H. van der Merwe, *Proc. R. Soc. London, Ser. A*, 1949, **198**, 216.
8 J. W. Matthews and A. E. Blakeslee, *J. Cryst. Growth*, 1974, **27**, 118–125.
9 S. C. Ying, *Phys. Rev. B*, 1971, **3**, 4160–4171.
10 A. D. Novaco and J. P. McTague, *Phys. Rev. Lett.*, 1977, **38**, 1286.
11 A. Koma and K. Yoshimura, *Surf. Sci.*, 1986, **174**, 556–560.
12 *Handbook of layered materials*, ed. S. M. Auerbach, K. A. Carrado and P. K. Dutta, Marcel Dekker, Inc., New York, 2004.
13 Y. Kuwahara, *Phys. Chem. Miner.*, 2001, **28**, 1–8.
14 B. S. Mitchell, *An Introduction to Materials Engineering and Science: For Chemical and Materials Engineers*, Wiley, New York, 2008.
15 W. Jaegermann, A. Klein and C. Pettenkofer, *Electronic Properties of Van der Waals-Epitaxy Film and Interfaces*, ed. H. P. Hughes and H. I. Starnberg, Springer, Netherlands, 2002, vol. 24, pp. 317–402.
16 A. Koma, K. Saiki and Y. Sato, *Appl. Surf. Sci.*, 1989, **41–42**, 451–456.
17 C. Hammond, A. Back, M. Lawrence, K. Nebesny, P. Lee, R. Schlaf and N. R. Armstrong, *J. Vac. Sci. Technol., A*, 1995, **13**, 1768–1775.
18 T. Loher, Y. Tomm, C. Pettenkofer and W. Jaegermann, *Appl. Phys. Lett.*, 1994, **65**, 555–557.
19 T. Loher, Y. Tomm, A. Klein, D. Su, C. Pettenkofer and W. Jaegermann, *J. Appl. Phys.*, 1996, **80**, 5718–5722.
20 E. Wisotzki, A. Klein and W. Jaegermann, *Adv. Mater.*, 2005, **17**, 1173–1177.
21 W. Dang, H. Peng, H. Li, P. Wang and Z. Liu, *Nano Lett.*, 2010, **10**, 2870–2876.
22 Y. Liu, M. Weinert and L. Li, *Phys. Rev. Lett.*, 2012, **108**, 115501.
23 H. Peng, W. Dang, J. Cao, Y. Chen, D. Wu, W. Zheng, H. Li, Z.-X. Shen and Z. Liu, *Nat. Chem.*, 2012, **4**, 281–286.
24 H. Li, J. Cao, W. Zheng, Y. Chen, D. Wu, W. Dang, K. Wang, H. Peng and Z. Liu, *J. Am. Chem. Soc.*, 2012, **134**, 6132–6135.
25 P. Gehring, B. F. Gao, M. Burghard and K. Kern, *Nano Lett.*, 2012, **12**, 5137–5142.
26 J. M. Garcia, U. Wurstbauer, A. Levy, L. N. Pfeiffer, A. Pinczuk, A. S. Plaut, L. Wang, C. R. Dean, R. Buizza, A. M. van Der Zande, J. Hone, K. Watanabe and T. Taniguchi, *Solid State Commun.*, 2012, **152**, 975–978.
27 G. Lippert, J. Dabrowski, M. Lemme, C. Marcus, O. Seifarth and G. Lupina, *Phys. Status Solidi B*, 2011, **248**, 2619–2622.
28 Y. Shi, W. Zhou, A.-Y. Lu, W. Fang, Y.-H. Lee, A. L. Hsu, S. M. Kim, K. K. Kim, H. Y. Yang, L.-J. Li, J.-C. Idrobo and J. Kong, *Nano Lett.*, 2012, **12**, 2784–2791.
29 A. Koma, *J. Cryst. Growth*, 1999, **201–202**, 236–241.
30 M. I. B. Utama, F. J. Belarre, C. Magen, B. Peng, J. Arbiol and Q. H. Xiong, *Nano Lett.*, 2012, **12**, 2146–2152.
31 M. I. B. Utama, Q. Zhang, S. F. Jia, D. H. Li, J. B. Wang and Q. H. Xiong, *ACS Nano*, 2012, **6**, 2281–2288.
32 R. Schlaf, S. Tiefenbacher, O. Lang, C. Pettenkofer and W. Jaegermann, *Surf. Sci.*, 1994, **303**, L343–L347.
33 O. Lang, R. Schlaf, Y. Tomm, C. Pettenkofer and W. Jaegermann, *J. Appl. Phys.*, 1994, **75**, 7805–7813.
34 Y. J. Hong and T. Fukui, *ACS Nano*, 2011, **5**, 7576–7584.
35 M. I. B. Utama, Z. P. Peng, R. Chen, B. Peng, X. L. Xu, Y. J. Dong, L. M. Wong, S. J. Wang, H. D. Sun and Q. H. Xiong, *Nano Lett.*, 2011, **11**, 3051–3057.
36 C. M. Lieber, *Solid State Commun.*, 1998, **107**, 607–616.
37 W. Lu and C. M. Lieber, *J. Phys. D: Appl. Phys.*, 2006, **39**, R387–R406.

38 P. D. Yang, Y. Y. Wu and R. Fan, *Int. J. Nanosci.*, 2002, **1**, 1–39.
39 C. M. Lieber and Z. L. Wang, *MRS Bull.*, 2007, **32**, 99–108.
40 Y. N. Xia, P. D. Yang, Y. G. Sun, Y. Y. Wu, B. Mayers, B. Gates, Y. D. Yin, F. Kim and Y. Q. Yan, *Adv. Mater.*, 2003, **15**, 353–389.
41 M. Law, J. Goldberger and P. D. Yang, *Annu. Rev. Mater. Res.*, 2004, **34**, 83–122.
42 F. Glas, *Phys. Rev. B*, 2006, **74**, 121302.
43 K. Tomioka, J. Motohisa, S. Hara and T. Fukui, *Nano Lett.*, 2008, **8**, 3475–3480.
44 L. K. Kavanagh, *Semicond. Sci. Technol.*, 2010, **25**, 024006.
45 E. Ertekin, P. A. Greaney, D. C. Chrzan and T. D. Sands, *J. Appl. Phys.*, 2005, **97**, 114325.
46 Z. H. Wu, X. Y. Mei, D. Kim, M. Blumin and H. E. Ruda, *Appl. Phys. Lett.*, 2002, **81**, 5177–5179.
47 J. Motohisa, J. Noborisaka, J. Takeda, M. Inari and T. Fukui, *J. Cryst. Growth*, 2004, **272**, 180–185.
48 J. Noborisaka, J. Motohisa and T. Fukui, *Appl. Phys. Lett.*, 2005, **86**, 213102.
49 X. Zhang, V. G. Dubrovskii, N. V. Sibirev and X. Ren, *Cryst. Growth Des.*, 2011, **11**, 5441–5448.
50 S. Sburlan, A. Nakano and P. D. Dapkus, *J. Appl. Phys.*, 2012, **111**, 054907.
51 L. C. Chuang, M. Moewe, C. Chase, N. P. Kobayashi, C. Chang-Hasnain and S. Crankshaw, *Appl. Phys. Lett.*, 2007, **90**, 043115.
52 X.-Y. Bao, C. Soci, D. Susac, J. Bratvold, D. P. R. Aplin, W. Wei, C.-Y. Chen, S. A. Dayeh, K. L. Kavanagh and D. Wang, *Nano Lett.*, 2008, **8**, 3755–3760.
53 A. Biermanns, S. Breuer, A. Trampert, A. Davydok, L. Geelhaar and U. Pietsch, *Nanotechnology*, 2012, **23**, 305703.
54 K. Tomioka, M. Yoshimura and T. Fukui, *Nature*, 2012, **488**, 189–192.
55 C. D. Bessire, M. T. Björk, H. Schmid, A. Schenk, K. B. Reuter and H. Riel, *Nano Lett.*, 2011, **11**, 4195–4199.
56 J. Shi and X. Wang, *J. Phys. Chem. C*, 2010, **114**, 2082–2088.
57 M. H. Huang, S. Mao, H. Feick, H. Q. Yan, Y. Y. Wu, H. Kind, E. Weber, R. Russo and P. D. Yang, *Science*, 2001, **292**, 1897–1899.
58 I. Levin, A. Davydov, B. Nikoobakht, N. Sanford and P. Mogilevsky, *Appl. Phys. Lett.*, 2005, **87**, 103110.
59 H.-M. Kim, D. S. Kim, D. Y. Kim, T. W. Kang, Y.-H. Cho and K. S. Chung, *Appl. Phys. Lett.*, 2002, **81**, 2193–2195.
60 B. J. Ohlsson, M. T. Björk, A. I. Persson, C. Thelander, L. R. Wallenberg, M. H. Magnusson, K. Deppert and L. Samuelson, *Phys. E.*, 2002, **13**, 1126–1130.
61 T. Mårtensson, C. P. T. Svensson, B. A. Wacaser, M. W. Larsson, W. Seifert, K. Deppert, A. Gustafsson, L. R. Wallenberg and L. Samuelson, *Nano Lett.*, 2004, **4**, 1987–1990.
62 H. J. Fan, R. Scholz, M. Zacharias, U. Gosele, F. Bertram, D. Forster and J. Christen, *Appl. Phys. Lett.*, 2005, **86**, 023113.
63 A. K. Debnath, S. Samanta, A. Singh, D. K. Aswal, S. K. Gupta, J. V. Yakhmi, S. K. Deshpande, A. K. Poswal and C. Sürgers, *Phys. E.*, 2008, **41**, 154–163.
64 D. Li, J. Zhang and Q. H. Xiong, *ACS Nano*, 2012, **6**, 5283–5290.
65 D. Li, J. Zhang, Q. Zhang and Q. H. Xiong, *Nano Lett.*, 2012, **12**, 2993–2999.
66 Q. Zhang, X. Liu, M. I. B. Utama, J. Zhang, M. de la Mata, J. Arbiol, Y. Lu, T. C. Sum and Q. H. Xiong, *Nano Lett.*, 2012, **12**, 6420–6427.
67 K. Saiki, K. Ueno, T. Shimada and A. Koma, *J. Cryst. Growth*, 1989, **95**, 603–606.
68 R. Chen, M. I. B. Utama, Z. Peng, B. Peng, Q. H. Xiong and H. Sun, *Adv. Mater.*, 2011, **23**, 1404–1408.
69 Q. Zhang, J. Zhang, M. I. B. Utama, B. Peng, M. d. l. Mata, J. Arbiol and Q. H. Xiong, *Phys. Rev. B*, 2012, **85**, 085418.
70 M. I. B. Utama, M. de la Mata, C. Magen, J. Arbiol and Q. H. Xiong, *Adv. Funct. Mater.*, 2012, DOI: 10.1002/adfm.201202027.
71 E. Janik, J. Sadowski, P. Dluzewski, S. Kret, L. T. Baczewski, A. Petroutchik, E. Lusakowska, J. Wrobel, W. Zaleszczyk, G. Karczewski, T. Wojtowicz and A. Presz, *Appl. Phys. Lett.*, 2006, **89**, 133114.
72 J. Pan, M. I. B. Utama, Q. Zhang, X. F. Liu, B. Peng, L. M. Wong, T. C. Sum, S. J. Wang and Q. H. Xiong, *Adv. Mater.*, 2012, **24**, 4151–4156.
73 K. S. Novoselov, A. K. Geim, S. V. Morozov, D. Jiang, Y. Zhang, S. V. Dubonos, I. V. Grigorieva and A. A. Firsov, *Science*, 2004, **306**, 666–669.
74 Y.-J. Kim, J.-H. Lee and G.-C. Yi, *Appl. Phys. Lett.*, 2009, **95**, 213101.
75 B. Kumar, K. Y. Lee, H.-K. Park, S. J. Chae, Y. H. Lee and S.-W. Kim, *ACS Nano*, 2011, **5**, 4197–4204.
76 A. M. Munshi, D. L. Dheeraj, V. T. Fauske, D.-C. Kim, A. T. J. van Helvoort, B.-O. Fimland and H. Weman, *Nano Lett.*, 2012, **12**, 4570–4576.
77 M. de la Mata, C. Magen, J. Gazquez, M. I. B. Utama, M. Heiss, S. Lopatin, F. Furtmayr, C. J. Fernández-Rojas, B. Peng, J. R. Morante, R. Rurali, M. Eickhoff, A. Fontcuberta i Morral and Q. H. Xiong, *Nano Lett.*, 2012, **12**, 2579–2586.
78 R. A. Laudise and A. A. Ballman, *J. Phys. Chem.*, 1960, **64**, 688–691.
79 M. Shiojiri and C. Kaito, *J. Cryst. Growth*, 1981, **52**, 173–177.
80 S. Conesa-Boj, E. Russo-Averchi, A. Dalmau-Mallorqui, J. Trevino, E. F. Pecora, C. Forestiere, A. Handin, M. Ek, L. Zweifel, L. R. Wallenberg, D. Rüffer, M. Heiss, D. Troadec, L. Dal Negro, P. Caroff and A. Fontcuberta i Morral, *ACS Nano*, 2012, **6**, 10982–10991.
81 K. Ikejiri, F. Ishizaka, K. Tomioka and T. Fukui, *Nano Lett.*, 2012, **12**, 4770–4774.
82 E. Uccelli, J. Arbiol, C. Magen, P. Krogstrup, E. Russo-Averchi, M. Heiss, G. Mugny, F. Morier-Genoud, J. Nygård, J. R. Morante and A. Fontcuberta i Morral, *Nano Lett.*, 2011, **11**, 3827–3832.
83 R. S. Wagner and W. C. Ellis, *Appl. Phys. Lett.*, 1964, **4**, 89.
84 S. A. Morin and S. Jin, *Nano Lett.*, 2010, **10**, 3459–3463.
85 G. W. Sears, *Acta Metall.*, 1955, **3**, 361–366.
86 H. Y. Dang, J. Wang and S. S. Fan, *Nanotechnology*, 2003, **14**, 738–741.

87 J. S. Lee, M. I. Kang, S. Kim, M. S. Lee and Y. K. Lee, *J. Cryst. Growth*, 2003, **249**, 201–207.
88 E. A. Stach, P. J. Pauzauskie, T. Kuykendall, J. Goldberger, R. R. He and P. D. Yang, *Nano Lett.*, 2003, **3**, 867–869.
89 Z. W. Pan, Z. R. Dai and Z. L. Wang, *Science*, 2001, **291**, 1947–1949.
90 Z. L. Wang, *Annu. Rev. Phys. Chem.*, 2004, **55**, 159–196.
91 S. C. Liu and J. J. Wu, *J. Mater. Chem.*, 2002, **12**, 3125–3129.
92 Z. L. Wang, X. Y. Kong and J. M. Zuo, *Phys. Rev. Lett.*, 2003, **91**, 185502.
93 P. D. Yang and C. M. Lieber, *J. Mater. Res.*, 1997, **12**, 2981–2996.
94 X. Xu, Y. Zhao, E. J. Sie, Y. Lu, B. Liu, S. A. Ekahana, X. Ju, Q. Jiang, J. Wang, H. Sun, T. C. Sum, C. H. A. Huan, Y. P. Feng and Q. H. Xiong, *ACS Nano*, 2011, **5**, 3660–3669.
95 Q. H. Xiong, J. Wang, O. Reese, L. C. Lew Yan Voon and P. C. Eklund, *Nano Lett.*, 2004, **4**, 1991–1996.
96 Q. H. Xiong, G. Chen, H. R. Gutierrez and P. C. Eklund, *Appl. Phys. A: Mater. Sci. Process.*, 2006, **85**, 299–305.
97 Q. H. Xiong, R. Gupta, K. W. Adu, E. C. Dickey, G. D. Lian, D. Tham, J. E. Fischer and P. C. Eklund, *J. Nanosci. Nanotechnol.*, 2003, **3**, 335–339.
98 K. W. Adu, Q. H. Xiong, H. R. Gutierrez, G. Chen and P. C. Eklund, *Appl. Phys. A: Mater. Sci. Process.*, 2006, **85**, 287–297.
99 G. Chen, J. Wu, Q. Lu, H. R. Gutierrez, Q. H. Xiong, M. E. Pellen, J. S. Petko, D. H. Werner and P. C. Eklund, *Nano Lett.*, 2008, **8**, 1341–1346.
100 J. Wu, D. Zhang, Q. Lu, H. R. Gutierrez and P. C. Eklund, *Phys. Rev. B*, 2010, **81**, 165415.
101 B. Ketterer, E. Uccelli and A. Fontcuberta i Morral, *Nanoscale*, 2012, **4**, 1789–1793.
102 B. Ketterer, M. Heiss, M. J. Livrozet, A. Rudolph, E. Reiger and A. Fontcuberta i Morral, *Phys. Rev. B*, 2011, **83**, 125307.
103 T. C. Damen, S. P. S. Porto and B. Tell, *Phys. Rev.*, 1966, **142**, 570–574.
104 J. M. Calleja and M. Cardona, *Phys. Rev. B*, 1977, **16**, 3753–3761.
105 R. Cuscó, E. Alarcón-Lladó, J. Ibáñez, L. Artús, J. Jiménez, B. Wang and M. J. Callahan, *Phys. Rev. B*, 2007, **75**, 165202.
106 K. McGuire, Z. W. Pan, Z. L. Wang, D. Milkie, J. Menendez and A. M. Rao, *J. Nanosci. Nanotechnol.*, 2002, **2**, 499–502.
107 H. Lüth, *Phys. Rev. Lett.*, 1972, **29**, 1377–1379.
108 X. L. Xu, S. P. Lau, J. S. Chen, G. Y. Chen and B. K. Tay, *J. Cryst. Growth*, 2001, **223**, 201–205.
109 J. Tauc, R. Grigorov and A. Vancu, *Phys. Status Solidi B*, 1966, **15**, 627.
110 V. Srikant and D. R. Clarke, *J. Appl. Phys.*, 1998, **83**, 5447–5451.
111 Y. Gu, I. L. Kuskovsky, M. Yin, S. O'Brien and G. F. Neumark, *Appl. Phys. Lett.*, 2004, **85**, 3833–3835.
112 K. Vanheusden, W. L. Warren, C. H. Seager, D. R. Tallant, J. A. Voigt and B. E. Gnade, *J. Appl. Phys.*, 1996, **79**, 7983–7990.
113 B. Lin, Z. Fu and Y. Jia, *Appl. Phys. Lett.*, 2001, **79**, 943–945.
114 U. Ozgur, Y. I. Alivov, C. Liu, A. Teke, M. A. Reshchikov, S. Dogan, V. Avrutin, S. J. Cho and H. Morkoc, *J. Appl. Phys.*, 2005, **98**, 041301.
115 D. O. Dumcenco, Y. S. Huang, D. H. Kuo and K. K. Tiong, *J. Lumin.*, 2012, **132**, 1890–1895.
116 D. M. Bagnall, Y. F. Chen, Z. Zhu, T. Yao, S. Koyama, M. Y. Shen and T. Goto, *Appl. Phys. Lett.*, 1997, **70**, 2230–2232.
117 R. Venugopal, P.-I. Lin, C.-C. Liu and Y.-T. Chen, *J. Am. Chem. Soc.*, 2005, **127**, 11262–11268.
118 V. G. Plotnichenko, Y. A. Mityagin and L. K. Vodop'yanov, *Sov. Phys. Solid State*, 1977, **19**, 1584.
119 R. Beserman, *Solid State Commun.*, 1977, **23**, 323–327.
120 A. K. Arora and A. K. Ramdas, *Phys. Rev. B*, 1987, **35**, 4345–4350.
121 A. Gavini and M. Cardona, *Phys. Rev. B*, 1970, **1**, 672–682.
122 V. E. Mashchenko and V. M. Vantsan, *Opt. Spectrosc.*, 1978, **28**, 313.
123 G. Perna, V. Capozzi and M. Ambrico, *J. Appl. Phys.*, 1998, **83**, 3337–3344.
124 A. Fujishima, X. Zhang and D. A. Tryk, *Surf. Sci. Rep.*, 2008, **63**, 515–582.
125 A. Ennaoui, S. Fiechter, C. Pettenkofer, N. Alonso-Vante, K. Büker, M. Bronold, C. Höpfner and H. Tributsch, *Sol. Energy Mater. Sol. Cells*, 1993, **29**, 289–370.
126 Y. Xia, D. Qian, D. Hsieh, L. Wray, A. Pal, H. Lin, A. Bansil, D. Grauer, Y. S. Hor, R. J. Cava and M. Z. Hasan, *Nat. Phys.*, 2009, **5**, 398–402.
127 H. J. Zhang, C. X. Liu, X. L. Qi, X. Dai, Z. Fang and S. C. Zhang, *Nat. Phys.*, 2009, **5**, 438–442.
128 J. Y. Lao, J. G. Wen and Z. F. Ren, *Nano Lett.*, 2002, **2**, 1287–1291.
129 C. Cheng, B. Liu, H. Yang, W. Zhou, L. Sun, R. Chen, S. F. Yu, J. Zhang, H. Gong, H. Sun and H. J. Fan, *ACS Nano*, 2009, **3**, 3069–3076.
130 L. J. Lauhon, M. S. Gudiksen, D. Wang and C. M. Lieber, *Nature*, 2002, **420**, 57–61.
131 B. Tian, X. Zheng, T. J. Kempa, Y. Fang, N. Yu, G. Yu, J. Huang and C. M. Lieber, *Nature*, 2007, **449**, 885–889.
132 M. S. Gudiksen, L. J. Lauhon, J. Wang, D. C. Smith and C. M. Lieber, *Nature*, 2002, **415**, 617–620.
133 Y. K. A. Lau, D. J. Chernak, M. J. Bierman and S. Jin, *J. Mater. Chem.*, 2009, **19**, 934–940.
134 R. Viswanathan, J. Zasadzinski and D. Schwartz, *Science*, 1993, **261**, 449–452.
135 L. Vayssieres, *Adv. Mater.*, 2003, **15**, 464–466.
136 L. E. Greene, M. Law, J. Goldberger, F. Kim, J. C. Johnson, Y. Zhang, R. J. Saykally and P. Yang, *Angew. Chem., Int. Ed.*, 2003, **42**, 3031–3034.
137 G. Yu, A. Cao and C. M. Lieber, *Nat. Nanotechnol.*, 2007, **2**, 372–377.
138 A. Javey, S. Nam, R. S. Friedman, H. Yan and C. M. Lieber, *Nano Lett.*, 2007, **7**, 773–777.
139 D. S. Kim, R. Ji, H. J. Fan, F. Bertram, R. Scholz, A. Dadgar, K. Nielsch, A. Krost, J. Christen, U. Gösele and M. Zacharias, *Small*, 2007, **3**, 76–80.
140 Y. Wei, W. Wu, R. Guo, D. Yuan, S. Das and Z. L. Wang, *Nano Lett.*, 2010, **10**, 3414–3419.

